LIFE SCIENCES

A20 haploinsufficiency disturbs immune homeostasis and drives the transformation of lymphocytes with permissive antigen receptors

Christoph Schultheiß[1,2], Lisa Paschold[3], Alma Nazlie Mohebiany[4,5,6], Moritz Escher[3], Yogita Mallu Kattimani[4], Melanie Müller[4], Paul Schmidt-Barbo[1,2,7], Anna Mensa-Vilaró[8,9], Juan Ignacio Aróstegui[8,9,10], Guilaine Boursier[11], Claire de Moreuil[12], Timo Hautala[13], Edith Willscher[3], Hanna Jonas[3], Namuun Chinchuluun[3], Bianca Grosser[14], Bruno Märkl[14], Wolfram Klapper[15], Prasad Thomas Oommen[16], Katharina Gössling[16,17], Katrin Hoffmann[18], Gisa Tiegs[19], Felix Czernilofsky[20,21,22], Sascha Dietrich[20,21,22,23,24], Alexandra Freeman[25], Daniella M. Schwartz[26], Ari Waisman[4], Ivona Aksentijevich[27], Mascha Binder[1,2,7]*

Genetic *TNFAIP3* (A20) inactivation is a classical somatic lymphoma lesion and the genomic trait in haploinsufficiency of A20 (HA20). In a cohort of 34 patients with HA20, we show that heterozygous *TNFAIP3* loss skews immune repertoires toward lymphocytes with classical self-reactive antigen receptors typically found in B and T cell lymphomas. This skewing was mediated by a feed-forward tumor necrosis factor (TNF)/A20/nuclear factor κB (NF-κB) loop that shaped pre-lymphoma transcriptome signatures in clonally expanded B (*CD81*, *BACH2*, and *NEAT1*) or T (*GATA3*, *TOX*, and *PDCD1*) cells. The skewing was reversed by anti-TNF treatment but could also progress to overt lymphoma. Analysis of conditional *TNFAIP3* knock-out mice reproduced the wiring of the TNF/A20/NF-κB signaling axis with permissive antigen receptors and suggested a distinct regulation in B and T cells. Together, patients with the genetic disorder HA20 provide an exceptional window into A20/TNF/NF-κB–mediated control of immune homeostasis and early steps of lymphomagenesis that remain clinically unrecognized.

INTRODUCTION

Haploinsufficiency of A20 (HA20) is a severe childhood-onset inflammatory disease characterized by heterozygous germline loss-of-function (LOF) mutations in *TNFAIP3* (*1*, *2*). The clinical presentations vary widely but often consist in periodic fever episodes with systemic symptoms and elevated inflammatory markers in the blood. Inflammatory episodes may involve the skin, joints, gastrointestinal tract, or other organs. Overall presentation but especially the mucosal ulcers observed in patients with HA20 are a shared feature with Behçet's disease. A20—the protein encoded by *TNFAIP3*—is an ubiquitin-editing enzyme that is critical for the negative regulation of nuclear factor κB (NF-κB) downstream of antigen, Toll-like, and tumor necrosis factor (TNF) receptors. Thereby, it plays a crucial role in regulating the innate immune response and in controlling inflammation. While the disease is mainly driven by dysregulation of innate immune cells, heterozygous A20 LOF also affect adaptive immunity since A20 restricts proliferation of B and T cells (*3*, *4*). A20-deficient B cells are resistant to Fas-mediated cell death (*5*) and also exhibit a hyperactive phenotype including autoantibody production that may account for some of the symptoms observed in HA20 (*6*). In line with this, germline-inherited single-nucleotide polymorphisms in the *TNFAIP3* gene locus compromising A20 function confer susceptibility to autoimmune diseases, including systemic lupus erythematosus, rheumatoid arthritis, psoriasis, Sjögren's syndrome, diabetes, and autoimmune hepatitis (*7*–*9*). Somatic A20 LOF has been identified as disease driver across a variety of non-Hodgkin lymphomas. Diffuse large B cell lymphoma of activated B cell type (ABC DLBCL) and cutaneous T cell non-Hodgkin lymphoma mycosis fungoides (MF)/Sézary syndrome (SS) are perhaps the most prototypic entities with mono- or biallelic *TNFAIP3*

[1]Division of Medical Oncology, University Hospital Basel, Basel, Switzerland. [2]Laboratory of Translational Immuno-Oncology, Department of Biomedicine, University and University Hospital Basel, Basel, Switzerland. [3]Internal Medicine IV, Oncology/Hematology, Martin-Luther-University Halle-Wittenberg, Halle (Saale), Germany. [4]Institute for Molecular Medicine, University Medical Center, Johannes Gutenberg University Mainz, Mainz, Germany. [5]Microglia and Inflammation in Neurological Disorders (MIND) Lab, VIB Center for Molecular Neurology, VIB, Antwerp, Belgium. [6]Department of Biomedical Sciences, University of Antwerp, Antwerp, Belgium. [7]Collaborative Research Institute Intelligent Oncology (CRIION), Freiburg, Germany. [8]Department of Immunology, Hospital Clínic de Barcelona, Barcelona, Spain. [9]Institut d'Investigacions Biomèdiques August Pi i Sunyer, Barcelona, Spain. [10]School of Medicine, University of Barcelona, Barcelona, Spain. [11]Department of molecular and cytogenomics, Rare and Autoinflammatory Diseases Laboratory, CHU Montpellier, IRMB, University of Montpellier, INSERM, CEREMAIA, Montpellier, France. [12]Department of Internal Medicine, CHU Brest, Université de Bretagne Occidentale, Brest, France. [13]Research Unit of Biomedicine, University of Oulu and Department of Internal Medicine, Oulu University Hospital, Oulu, Finland. [14]Institute for Pathology, University Medical Center Augsburg, Augsburg, Germany. [15]Institute of Pathology, Hematopathology Section, and Lymph Node Registry, University Hospital Schleswig-Holstein, Campus Kiel, Kiel, Germany. [16]Department of Pediatric Oncology, Hematology, and Clinical Immunology, Medical Faculty, Center for Child and Adolescent Health, Heinrich Heine University Düsseldorf, Düsseldorf, Germany. [17]Department of Pediatrics, University Hospital Schleswig-Holstein, Kiel, Germany. [18]Institute for Human Genetics and Molecular Biology, Martin-Luther-University Halle-Wittenberg, Halle (Saale), Germany. [19]Institute for Experimental Immunology and Hepatology, University Medical Center Hamburg-Eppendorf, Hamburg, Germany. [20]Department of Medicine V, Hematology, Oncology, and Rheumatology, University of Heidelberg, Heidelberg, Germany. [21]European Molecular Biology Laboratory (EMBL), Heidelberg, Germany. [22]Molecular Medicine Partnership Unit (MMPU), Heidelberg, Germany. [23]Department of Translational Medical Oncology, National Center for Tumor Diseases (NCT) Heidelberg and German Cancer Research Center (DKFZ), Heidelberg, Germany. [24]Department of Hematolgy, Oncology, and Immunolgy, University Hospital of Düsseldorf, Düsseldorf, Germany. [25]Laboratory of Clinical Immunology, National Institute of Allergy and Infectious Diseases, NIH, Bethesda, MD, USA. [26]Division of Rheumatology and Clinical Immunology, University of Pittsburgh, Pittsburgh, PA, USA. [27]Inflammatory Disease Section, National Human Genome Research Institute, National Institutes of Health, Bethesda, MD, USA.
*Corresponding author. Email: mascha.binder@unibas.ch

mutations (*10*–*15*). As in other lymphomas, these mutations are believed to disrupt tolerance checkpoints permitting lymphocytes to evade growth control (*16*–*18*). However, it remains underexplored how single recurrent lymphoma mutations turn signals resulting from antigen receptor engagement into proliferation or alternatively prevent self-antigen–induced clonal deletion.

In the work presented here, we study a unique cohort of 34 individuals with HA20 with a focus on lymphocyte dysregulation. We show that loss of A20 creates a distinct interactome with "permissive" lymphoma antigen receptor configurations that results in the reversible TNF-driven expansion of selected clonotypes in patients with HA20. By engineering lymphoid or myeloid lineage–specific deletion of *TNFAIP3* in mouse models and by manipulation of lymphoma cell lines, we dissect the cell-intrinsic and -extrinsic loops of the A20/TNF/NF-κB axis determining B and T cell homeostasis versus clonal outgrowth. Overall, these data provide valuable insight into the biological trajectory from healthy lymphocytes to lymphoma at the same time pointing at the lymphoma risk and potential mitigation strategies in patients with HA20.

RESULTS

Patients with HA20 show skewing of T and B cell immune repertoires

Given the importance of somatic *TNFAIP3* LOF mutations in lymphoma, we hypothesized that lymphocyte repertoire composition in patients with HA20 may reveal unprecedented insight into the pleiotropic effects of A20 on lymphoid cells. Therefore, we systematically analyzed peripheral blood B and T cell repertoires in a cohort of 34 individuals with HA20, 19 thereof as part of six affected families (table S1), using immunoglobulin heavy chain (IGH) and T cell receptor β chain (TRB) repertoire sequencing (Fig. 1A). Compared to healthy individuals, immune repertoires of patients with HA20 were restricted with overall higher clonality and lower diversity and richness (Fig. 1B). The metrics shifts were more pronounced for the IGH repertoire than for the TRB repertoire. The rate of IGHV somatic hypermutation was comparable to controls indicating no severe maturation defect or antigenic driver in HA20 B cells (Fig. 1B). To detect HA20-associated biases in the T and B cell immune repertoires, we performed principal component analysis (PCA) of V gene usage. TRBV and IGHV gene usage was substantially skewed (Fig. 1C). The most frequently used TRBV gene was TRBV20-1, which was strongly enriched compared to immune repertoires from healthy individuals. In the B cell repertoire, we found increased usage of IGHV3-23 and IGHV4-34, the latter being known for its reactivity with self-antigen (Fig. 1D). In addition, IGHV3-7 and, to a lesser extent, IGHV2-5 and IGHV3-74 were enriched in HA20 repertoires. Together, these data suggest the selective expansion of B and T lymphocytes with distinct antigen receptor rearrangements in individuals with germline LOF *TNFAIP3* mutations.

Skewed HA20 immune repertoires encompass antigen receptor signatures of *TNFAIP3*-mutant lymphomas

Next, we asked whether the HA20-specific immune repertoire skewing was directed toward antigen receptor genes typically used by *TNFAIP3*-mutant lymphomas. To test this, we studied antigen receptor profiles in two lymphoma entities that frequently harbor *TNFAIP3* mutations, namely DLBCL of ABC type and MF/SS. In these cohorts, 21 of 66 ABC DLBCL cases (Fig. 1E) and 9 of 27 MF/SS cases (Fig. 1F) (dbGAP, accession number phs000859) had *TNFAIP3* mutations. In *TNFAIP3*-mutant ABC DLBCL, a variety of different *TNFAIP3* alterations were found and almost one-third of all cases had biallelic inactivations (Fig. 1E and table S2). In *TNFAIP3*-mutant MF/SS, the prevailing lesion was a monoallelic *TNFAIP3 c.380 T > G* (p.Phe127Cys; NCBI: NM_006290.4) alteration (Fig. 1F and table S2). To determine the malignant lymphoma's antigen receptor sequence, we performed next-generation sequencing (NGS) of the *IGH* locus in our ABC DLBCL cases and extracted the dominant *TRB* sequence from RNA-sequencing (RNA-seq) data in the MF/SS cohort. This analysis demonstrated that the majority of *TNFAIP3*-mutant ABC DLBCL or MF/SS lymphomas used IGHV4-34 (57%) or TRBV20-1 (33%), respectively (Fig. 1, F and G). While these two genes were among the V genes most frequently expanded in HA20 B and T cell immune repertoires, we did not detect clonotypes with identical IGHV4-34 or TRBV20-1 receptor configurations shared between patients with lymphoma. Together, these data suggest that the penetrance and expressivity of *TNFAIP3* mutations on the immune repertoire level is linked to the expression of distinct permissive antigen receptors.

The transcriptome of healthy B cells expressing IGHV4-34–encoded antigen receptors is closely linked to *TNFAIP3*

We next focused on the B lineage and asked whether autonomous, antigen-independent B cell receptor (BCR) properties contributed to the enrichment of distinct V genes in *TNFAIP3* LOF settings. We randomly selected two IGHV4-34–encoded clonotypic BCR derived from patients with ABC DLBCL as proxy to test this using the murine triple knock-out (TKO) system (*19*). When ectopically expressing these BCR in TKO cells, we did not observe autonomous signaling and equal levels of Ca^{2+} mobilization upon anti–immunoglobulin M (IgM) stimulation compared to an unrelated control BCR (Fig. 2A) (*20*). These data did not suggest autonomous signaling or differential responses to receptor engagement as inherent distinguishing feature of IGHV4-34–encoded BCR. We next tested the hypothesis that B cells with IGHV4-34–encoded BCR share characteristic A20-related signaling properties that render them more permissive for *TNFAIP3* LOF mutations. To this end, we isolated peripheral $CD19^+$ cells with and without IGHV4-34–encoded BCRs from a healthy individual (male, 24 years old) and subjected them to 5′ single-cell RNA (scRNA) and paired BCR sequencing. This yielded 3536 IGHV4-34^+ and 8726 IGHV4-34^- B cells. Dimensionality reduction and embedding using Uniform Manifold Approximation and Projection (UMAP) after integration of both datasets showed that the polyclonal IGHV4-34^+ and IGHV4-34^- populations shared all major B cell compartments distributed across eight clusters (Fig. 2B). While there were only subtle differences in the proportion of naïve/mature and classical memory subsets, IGHV4-34^+ cells were enriched in B cells with an atypical-like signature (*FCRL3*, *FCRL5*, *ITGAX*, *SOX5*, and lack of *CD27*) (*21*–*24*) (Fig. 2B) and contained less post-class switch isotypes (Fig. 2C). IGHV4-34^+ cells showed substantially lower *TNFAIP3* expression with *TNFAIP3* being one of the top 50 differentially regulated genes in an unsupervised analysis (Fig. 2D). Notably, we observed the same but less pronounced pattern in IGHV3-7 and IGHV3-23 expressing B cells but not for any other of the 32 IGHV family classes that were sufficiently covered in the non–IGHV4-34 dataset (fig. S1). To exclude

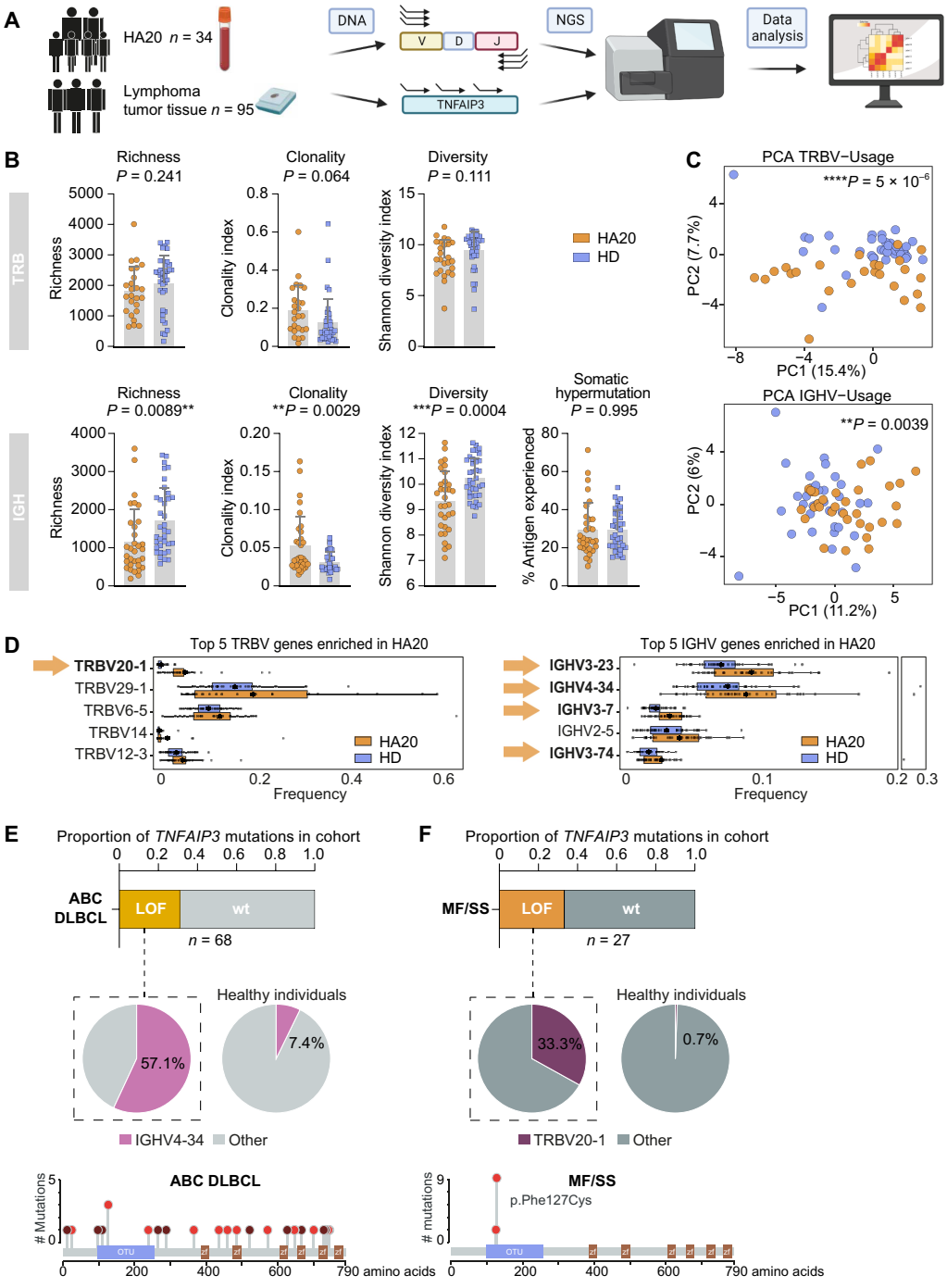

Fig. 1. B and T cell receptors in blood lymphocytes of patients with HA20 and in lymphoma cohorts. (**A**) Schematic representation of sequencing approach. Created with Biorender.com. (**B**) Mean (±SD) richness, clonality, Shannon diversity, and hypermutation rate for the productive IGH and TRB repertoires from patients with HA20 ($n = 34$) compared to healthy individuals (HD; $n = 36$). Statistical analysis: Unpaired two-sided t test. (**C**) PCA of TRBV and IGHV gene usage in patients with HA20 ($n = 34$) and HDs (n = 36). Statistical analysis: Pillai-Bartlett test of multivariate analysis of variance (MANOVA) of all principal components. (**D**) Median frequency of TRBV or IGHV gene usage for the top five V gene families in patients with HA20 ($n = 34$) and HDs ($n = 36$). Arrows indicate V genes commonly found in lymphoma clones. The boxes span the 25th to 75th percentiles; whiskers, the 10th to 90th percentile. (**E**) Proportion of patients with somatic *TNFAIP3* mutations in the analyzed cohort of patients with diffuse large B cell lymphoma of activated B cell type (ABC DLBCL) ($n = 68$) and frequency of lymphoma clones with IGHV4-34 rearranged antigen receptors in *TNFAIP3*-mutated patients as compared to healthy donor (HD) immune repertoires ($n = 36$). Moreover, position and number of identified *TNFAIP3* mutations in the ABC DLBCL cohort are shown. Red dots indicate missense mutations, dark dots nonsense or frameshifts. The TNFAIP3 OTU (ovarian tumor) domain mediates deubiquitinase activity, and the A20-type zinc fingers (ZF) mediates ubiquitin ligase activity. (**F**) Proportion of patients with somatic *TNFAIP3* mutations in the analyzed MF/SS cohort ($n = 27$) and frequency of peripheral lymphoma clones with TRBV20-1 rearranged antigen receptors in *TNFAIP3*-mutated patients as compared to peripheral blood from HDs ($n = 36$). Position and number of identified *TNFAIP3* mutations in the MF/SS cohort are shown. $^{**}P < 0.01$; $^{***}P < 0.001$; $^{****}P < 0.0001$.

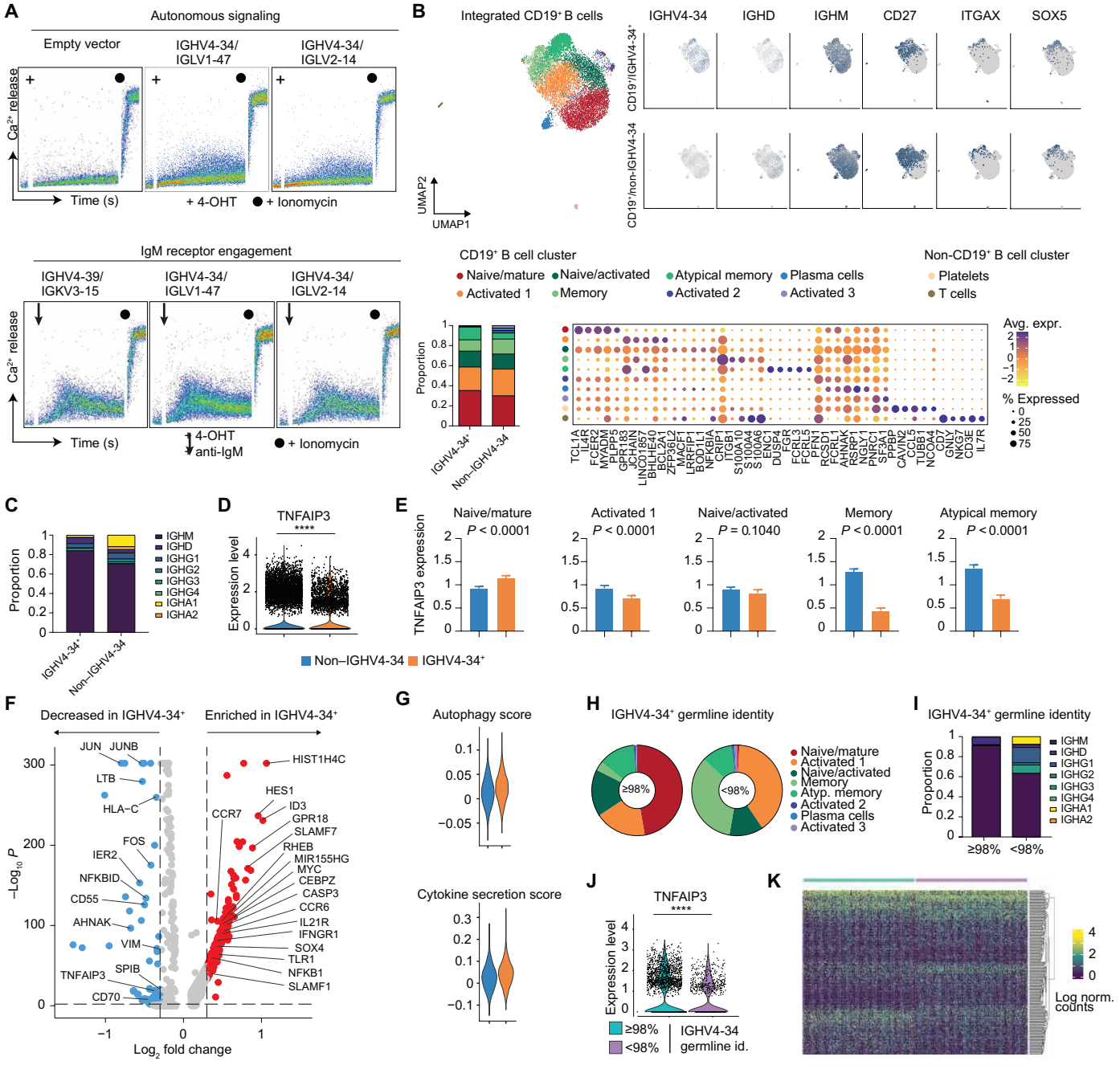

Fig. 2. The signaling capacity and transcriptome of B cells with IGHV4-34–encoded antigen receptors. (**A**) Ca^{2+} flux measurements in TKO cells transduced with the indicated lymphoma-derived IGHV4-34 or control BCRs after induction with 4-hydroxytamoxifen (4-OHT) and anti-IgM antibody. (**B**) UMAP projection of scRNA-seq data of IGHV4-34$^+$ and non–IGHV4-34 B cells of a healthy individual. Cell proportions per cluster are shown as stacked bar plot and the top five differentially expressed genes per cluster as dot plot. (**C**) Proportion of class-switched cells per cluster. (**D**) *TNFAIP3* expression in all IGHV4-34$^+$ and non–IGHV4-34 B cells. Statistics: Mann-Whitney *U* test. (**E**) *TNFAIP3* expression in IGHV4-34$^+$ and non–IGHV4-34 clusters with at least 200 cells. Statistics: Mann-Whitney *U* test. (**F**) Volcano plot showing differential gene expression between IGHV4-34$^+$ and non–IGHV4-34 B cells. Genes were considered differentially expressed with an adjust $P < 0.01$. (**G**) Autophagy and cytokine secretion score in IGHV4-34$^+$ and non–IGHV4-34 B cells. (**H**) Proportion of antigen-experienced and naïve IGHV4-34 B cells. IGHV4-34 encoded BCRs with ≤98% sequence identity to the germline V gene are considered antigen-experienced. (**I**) Proportion of class-switched IGHV4-34$^+$ B cells dependent on antigen experience. (**J**) *TNFAIP3* expression in all IGHV4-34$^+$ B cells depending on antigen experience. Statistics: Mann-Whitney *U* test. (**K**) Heatmap of top 50 differentially expressed genes in all IGHV4-34$^+$ B cells depending on IGHV4-34 germline identity. ****$P < 0.0001$.

that the reduced *TNFAIP3* transcription in IGHV4-34$^+$ cells was an effect of anti–IGHV4-34 antibody binding during sorting, we subjected a set of 22,912 CD19-sorted B cells from two additional healthy individuals (52-year-old female and 62-year-old male) to scRNA-seq. Here, we observed the same reduced *TNFAIP3* transcript levels in IGHV4-34$^+$ cells (fig. S2). In IGHV4-34–sorted cells, the reduced *TNFAIP3* expression pattern was mainly derived from expression differences in the classical memory (*CD27*, lack of *IGHD*) and the atypical-like B cell compartments (Fig. 2, D and E). In addition, IGHV4-34$^+$ cells had higher expression of *NFKB1* as well as NF-κB activators (*SLAMF1*, *SLAMF7*, and *TLR1*) and NF-κB downstream targets (e.g., *MYC*, *MIR155HG, CCR7*, and *ID3*), while the NF-κB inhibitor *NFKBID* was down-regulated (Fig. 2F). IGHV4-34$^+$ cells were also characterized by slightly higher gene expression scores for autophagy and proinflammatory cytokine secretion (Fig. 2G). Next, we tested for gene expression differences depending on antigen experience of the BCR in the IGHV4-34$^+$ population. In line with the receptor status, IGHV4-34$^+$ cells with near germline receptor configuration (≥98% identity) had higher proportion of cells expressing naïve B cell markers (*TCL1A*) (Fig. 2H) and pre-switch isotypes (Fig. 2I), while antigen-experienced IGHV4-34$^+$ cells (BCR configuration with less than 98% germline identity) were enriched in classical memory markers (CD27) (Fig. 2H) and post-switch isotypes (Fig. 2I). Notably, antigen-experienced IGHV4-34 BCRs had lower levels of *TNFAIP3* (Fig. 2J) but no substantial differences in global gene expression besides lineage-specific memory markers (Fig. 2K). These data suggest that the reduced *TNFAIP3* expression levels in IGH4-34$^+$, IGHV3-7$^+$, and IGHV3-23$^+$ subsets may render them more sensitive to the effects induced by heterozygous loss of *TNFAIP3* as compared to B cell populations with other BCR configurations.

Therapeutic TNF antagonism reverses lymphoma-like repertoire skewing in HA20

Given the pivotal role of A20 for NF-κB signaling, we asked whether molecular mediators of this pathway promote the observed repertoire effects in HA20. One of the key NF-κB targets that trigger a positive feedback loop is the TNF. We reasoned that, if TNF drives repertoire skewing in HA20, therapeutic TNF blockade would reverse this effect and result in repertoire normalization. To study this, we longitudinally assessed immune repertoires in patient HA20-1 on treatment with the TNF antagonist infliximab. Before treatment initiation, this patient showed classical A20 deficiency with constitutive NF-κB activation (Fig. 3A) and excessive proinflammatory cytokine elevations, especially TNF (Fig. 3B). At that time, the patient also had reduced B cell repertoire richness and diversity in line with the repertoire metrics of our entire HA20 patient cohort (Figs. 3C and 1B). Upon initiation of therapeutic TNF antagonism, patient HA20-1 normalized her B cell repertoire metrics to richness and diversity measures characteristic of blood B cells of healthy

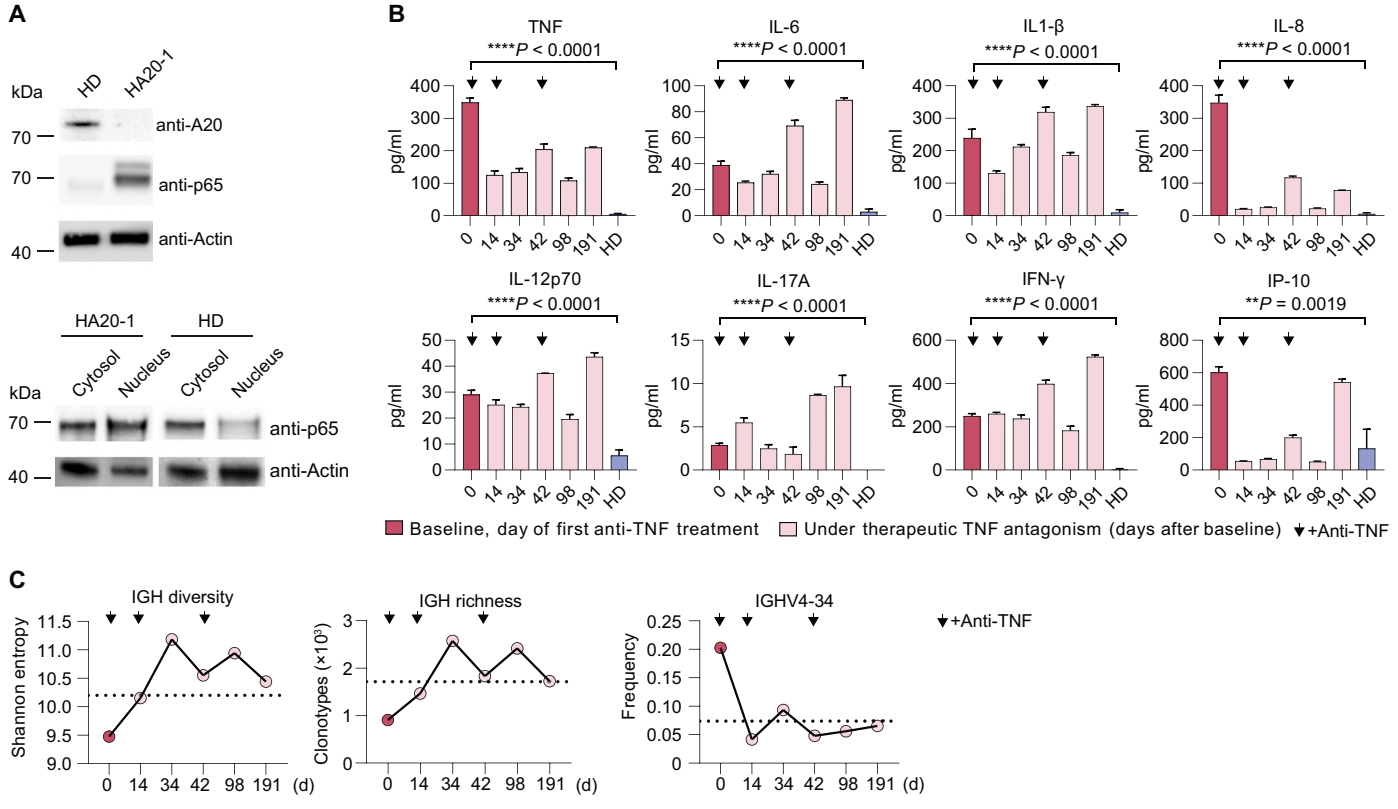

Fig. 3. Effects of TNF antagonism on cytokine dysregulation and immune repertoire skewing in HA20. (**A**) Immunoblotting of A20 and NF-κB status in PBMCs from patient HA20-1 and a healthy individual (HD). NF-κB activation was assessed by nuclear translocation of p65. (**B**) Mean (±SD) cytokine plasma levels of patient HA20-1 at initial presentation (day 0) and at indicated follow-up time points as compared to six HDs. Arrows indicate sampling days with subsequent infliximab application. All individuals were measured as technical duplicate. Statistics: ordinary one-way ANOVA. (**C**) Longitudinal monitoring of immune repertoire diversity, richness, and IGHV4-34 usage in patient HA20-1 at initial presentation and on therapeutic TNF antagonism (infliximab) as compared to six HD. $^{**}P < 0.01$; $^{****}P < 0.0001$.

individuals (Fig. 3C). Moreover, before treatment initiation, this patient showed strong polyclonal expansion of IGHV4-34^{+} B cells that made up almost 20% of the B cell repertoire (Fig. 3C). On TNF blockade, IGHV4-34–expressing B cells normalized to a repertoire frequency typically found in healthy individuals (Fig. 3C). These data suggest that TNF is an essential mediator of A20 loss in lymphocyte repertoire skewing.

The proliferative effects of A20-loss are mediated by a positive autocrine TNF feedback loop

We further explored whether TNF-induced proliferative effects mediated by NF-κB were also present in the setting of somatic A20 loss in lymphomas. For these studies, we chose the lymphoma cell lines OCI-Ly3 and JVM-2 harboring a *TNFAIP3* wild-type gene and RI-1, SU-DHL-2, and Karpas-1106p with a mutant *TNFAIP3*. OCI-Ly3 and RI-1 cell lines expressed typical lymphoma IGHV genes (IGHV4-34 and IGHV3-7, respectively). A20 protein abundancy mirrored the *TNFAIP3* mutation status (Fig. 4A). A20-deficient cells displayed nuclear enrichment of the NF-κB subunit p65 (Fig. 4B) as well as much higher quantities of secreted TNF than OCI-Ly3 or JVM-2 (Fig. 4C). TNF antagonism with infliximab resulted in the selective reduction of RI-1, SU-DHL-2, and Karpas-1106p proliferation (Fig. 4D) but not cell viability (Fig. 4E). Reconstitution of A20 in RI-1 cells did not affect p65 levels (Fig. 4F) but reversed nuclear enrichment (Fig. 4G) and blocked TNF secretion (Fig. 4H), which was accompanied by reduced proliferation that could not be reversed by TNF antagonism (Fig. 4I). RNA-seq revealed broad down-regulation of NF-κB, Janus kinase–signal transducers and activators of transcription (JAK-STAT), and interferon pathways including factors related to BCR-mediated signaling (*CD82*, *KLF3*, and *FOXO1*), differentiation (FCRL5), as well as immune checkpoints (*PDCD1*, *LAG3*, *TIGIT*, and *TOX*) (Fig. 4, J and K). Reconstitution of A20 resulted in up-regulation of *GATA3*, which is known to repress proliferation in B cells (Fig. 4J). Next, we sought to corroborate the direct role of NF-κB for mediating the observed TNF secretion and proliferation patterns. For this, we targeted NF-κB in the A20-deficient cell lines RI-1 and Karpas-1106p using pyrrolidinedithiocarbamate (PDTC) (*25*). We chose those two models to cover the complete spectrum of TNF secretion. While the PDTC-induced inactivation resulted in reduced TNF secretion in both models (Fig. 4L), the decrease was much more pronounced in RI-1 cells that generally showed the highest rates of TNF secretion (Fig. 4, C and L). Last, we tested whether TNF can drive its own secretion in selected cell models. As shown in Fig. 4M, TNF stimulation of A20-proficient (OCI-Ly3) or A20-deficient cells (RI-1) resulted in TNF secretion in both cases. Notably, the A20-deficient RI-1 cells secreted substantially higher amounts of TNF as compared to their counterparts with reconstituted A20, which showed a TNF secretion pattern similar to OCI-Ly3 cells (Fig. 4M). Together, these data suggest that the proliferation of A20-deficient lymphoma cells can be increased by a feed-forward loop of auto-/paracrine TNF mediated by NF-κB.

Systemic TNF elevation shapes *TNFAIP3* wild-type lymphocyte repertoires in mice

We next asked whether excessive systemic TNF alone—in the absence of lymphocyte-intrinsic A20 deficiency–can shape lymphocyte repertoires. To test this in an HA20-like setting, we choose a mouse model with selective deletion of *TNFAIP3* in the monocyte/macrophage compartment, which is the main source of systemic TNF in myeloid *TNFAIP3*-KO models (*26*, *27*). To this end, we crossed A20$^{fl/fl}$ mice to Cx3cr1-Cre$^{ERT2/+}$ mice (termed hereafter A20$^{Cx3cr1\text{-}KO}$), which allows tamoxifen–inducible Cre expression driven by the *Cx3cr1* promoter in the mononuclear phagocyte compartment, including monocytes, macrophages, and microglia (Fig. 5A) (*28*). In line with previous gene expression data from this model (*29*), A20$^{Cx3cr1\text{-}KO}$ mice showed substantially higher TNF plasma levels than A20$^{fl/fl}$ mice (Fig. 5B). There was also a trend toward higher interleukin-6 (IL-6) levels (Fig. 5B) but no broad dysregulation of cytokines as observed in HA20 (Fig. 3B). Peripheral T cell repertoires derived from blood, spleen, and lymph nodes were considerably more clonal in A20$^{Cx3cr1\text{-}KO}$ mice, while B cell repertoires from the same tissues appeared rather unaffected (Fig. 5C). Thymic T cell repertoires were used as controls. These showed low clonality, which was unaffected by an A20-deficient monocyte/macrophage compartment (Fig. 5C). The B cell repertoires of A20$^{Cx3cr1\text{-}KO}$ mice also showed lower repertoire richness and a trend toward increased clonality although less pronounced than in the T cell repertoire (Fig. 5C). Anti-TNF treatment normalized repertoire richness and clonality to the levels observed in A20 wild-type mice (Fig. 5C). PCA showed that the increase in peripheral T cell repertoire clonality reflected the skewing toward selective expansion of T cells with TRBV17, TRBV5, and TRBV12-1 receptor configurations (Fig. 5D), which contracted again under anti-TNF treatment (Fig. 5E).

Next, we generated mice with B cell–restricted A20 deletion by crossing A20$^{fl/fl}$ mice to CD19-Cre$^{+/-}$ mice (termed hereafter A20$^{CD19\text{-}KO}$) (Fig. 5A) (*6*). These mice also showed a trend toward elevated TNF plasma levels as compared to the control mice, but these elevations were substantially lower and not general as observed in the A20$^{Cx3cr1\text{-}KO}$ mice (Fig. 5F). Other cytokines were not affected (Fig. 5F). We detected neither T nor B cell repertoire shifts in A20$^{CD19\text{-}KO}$ mice (Fig. 5G). Together, these results suggest that systemic TNF can induce repertoire shifts in peripheral T cells and, to a lesser degree, also in B cells given that its systemic levels are sufficiently elevated.

HA20 lymphocytes can transform into lymphoma cells

Given the observed effects of A20 loss in permissive lymphocytes, we reasoned that patients with HA20 may be at risk for lymphoma development. Since HA20 is a rare and only recently described monogenetic disorder, no systematic screening for lymphoma risk associations has been performed. In our cohort, no standardized monitoring was performed, with some patients having only one or few contacts with the physician contributing patients to this cohort. Despite this, two patients from our cohort of 34 individuals developed lymphoma in the course of their disease. Patient HA20-15 has a chromosomal deletion in 6q23.3, which encompasses *TNFAIP3* and developed marginal zone lymphoma, and patient HA20-14 was diagnosed with DLBCL in the course of his otherwise mild inflammatory disease. Molecular analysis of lymphoma tissue from patient HA20-14 showed two second genetic hits in addition to his previously identified germline *TNFAIP3* c.503G > A (p.Trp168*) mutation: an additional *TNFAIP3* c.1880_1881delGT (p.Cys627fs) mutation along with an *MYD88* c.617C > G (p.Ser206Cys) mutation (Fig. 6A). The

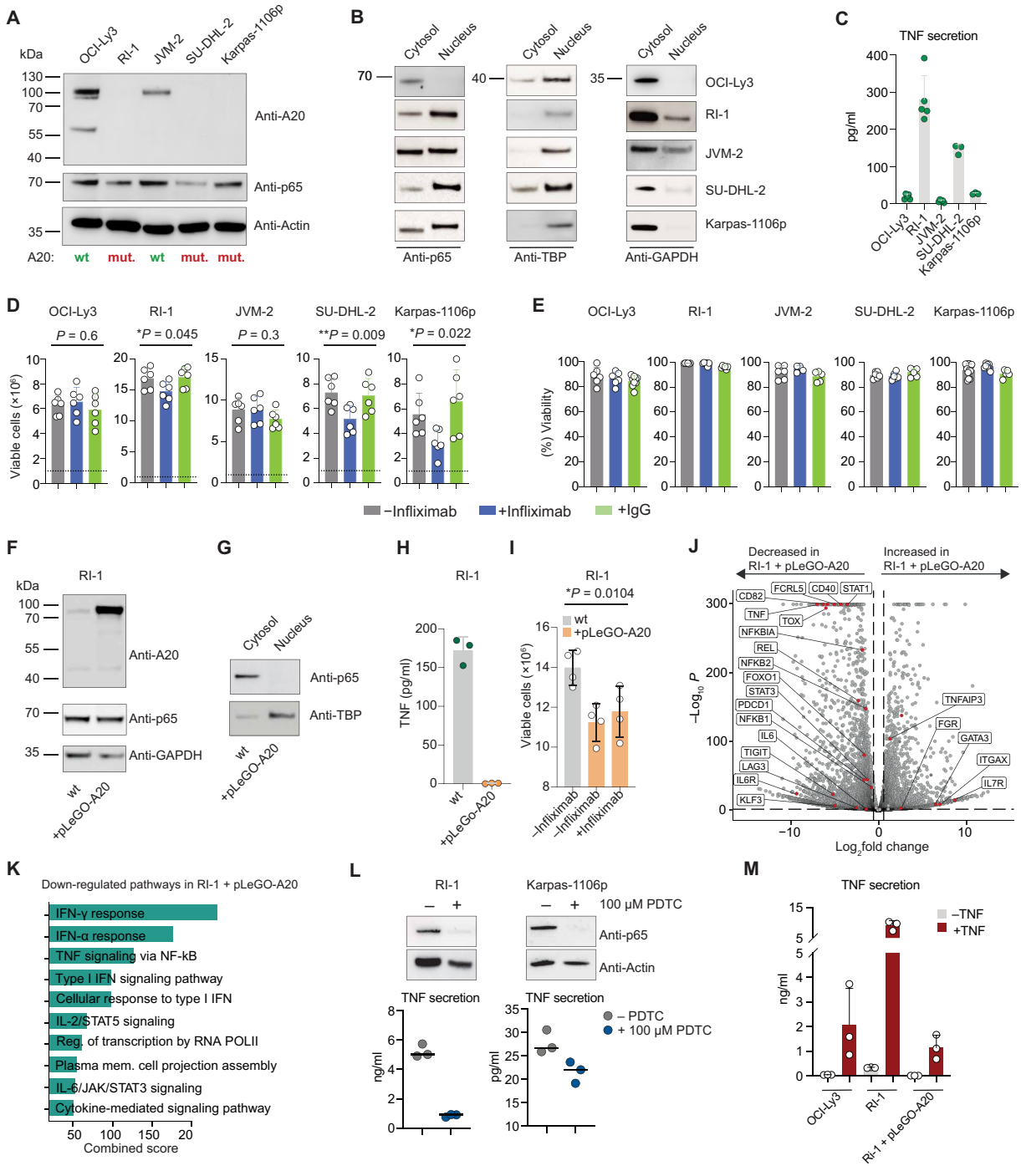

Fig. 4. A20–NF-κB–dependent TNF secretion drives proliferation of in vitro cell models of lymphoma. (**A**) Immunoblotting of A20 and NF-κB p65 in whole-cell extract from B cell lymphoma cell lines. (**B**) Immunoblotting of NF-κB p65 in cytosolic and nuclear fractions of indicated cell lines. TBP and glyceraldehyde-3-phosphate dehydrogenase (GAPDH) served as loading controls. (**C**) Quantification of mean (±SD) TNF secretion by indicated cell lines ($n = 3$ to 4 biological replicates). (**D**) Mean (±SD) proliferation and (**E**) viability of indicated cell lines ($n = 6$ biological replicates) after 72 hours of incubation with anti-TNF antibody infliximab or human IgG (Intratect). Dotted lines represent seeded cell number. (**F**) Immunoblotting of A20 and NF-κB p65 after lentiviral transduction of A20 in RI-1 cells. (**G**) Immunoblotting of NF-κB p65 in cytosolic and nuclear fractions after A20 reconstitution in RI-1 cells. (**H**) Mean (±SD) TNF secretion after lentiviral transduction of A20 in RI-1 cells ($n = 3$ biological replicates). (**I**) Mean (±SD) proliferation of A20-overexpressing RI-1 cells in the presence of infliximab ($n = 4$ biological replicates). Statistics: one-way ANOVA. (**J**) Volcano plot showing differential gene expression between RI-1 wt and RI-1 + pLeGO-A20 as determined by RNA-seq performed in duplicates. Genes were considered differentially expressed with an adjust $P < 0.01$ and $\log_2$ fold change > 1. (**K**) Top down-regulated signaling pathways in RI-1 + pLeGO-A20 cells. All adjusted P values < 0.0001. (**L**) Immunoblotting of NF-κB p65 in whole-cell extract and quantification of secreted TNF after incubation with 100 μM PDTC for 1 hour ($n = 3$ biological replicates). (**M**) Quantification of mean (±SD) TNF secretion after stimulation with 100 ng/ml recombinant TNF for 1 hour ($n = 3$ biological replicates). $^*P < 0.05$; $^{**}P < 0.01$.

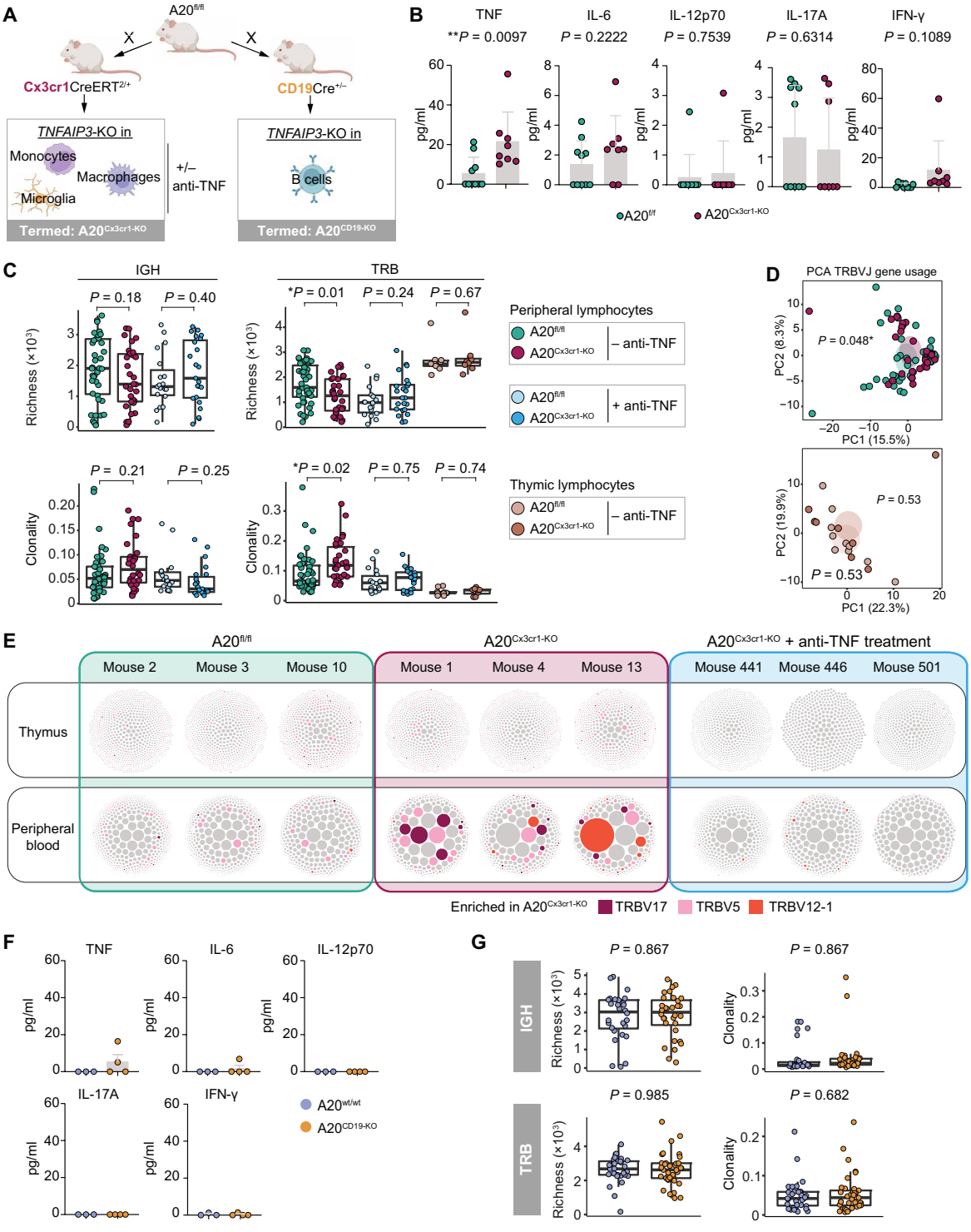

Fig. 5. *TNFAIP3* gene targeting in the mononuclear phagocyte but not CD19 compartment increases plasma TNF and shapes the peripheral lymphocyte compartments. (**A**) Schematic representation of mice breedings and treatments. Created with Biorender.com. (**B**) Quantification of mean (±SD) plasma cytokine levels in $A20^{Cx3cr1\text{-}KO}$ ($n = 8$) and $A20^{fl/fl}$ mice ($n = 10$). Statistics: two-sided *t* test. (**C**) Mean (±SD) immune repertoire metrics from peripheral lymphocytes (peripheral blood, spleen, and lymph nodes) and thymic lymphocytes of $A20^{Cx3cr1\text{-}KO}$ ($n = 8$) and $A20^{fl/fl}$ mice ($n = 11$). Injection with anti-TNF antibody as indicated in $A20^{Cx3cr1\text{-}KO}$ ($n = 6$) and $A20^{fl/fl}$ mice ($n = 5$). Statistics: two-sided *t* test. (**D**) PCA of TRBV gene distribution in peripheral and thymic lymphocytes of $A20^{fl/fl}$ ($n = 11$) and $A20^{Cx3cr1\text{-}KO}$ ($n = 8$). Statistics: Pillai-Bartlett test of MANOVA of all principal components. (**E**) Visualization of T cell clonotypes in indicated compartments from selected individual mice. Enriched clonotypes marked in colors with corresponding TRBV genes. (**F**) Quantification of mean (±SD) plasma cytokine levels of $A20^{CD19\text{-}KO}$ ($n = 3$) and $A20^{fl/fl}$ mice ($n = 4$). (**G**) Mean (±SD) immune repertoire metrics from peripheral lymphocytes (peripheral blood, spleen, and lymph nodes) lymphocytes of $A20^{CD19\text{-}KO}$ ($n = 7$) and $A20^{fl/fl}$ mice ($n = 8$). Statistics: two-sided *t* test. $^*P < 0.05$; $^{**}P < 0.01$.

malignant clone expressed IGHV3-23, one of the preferentially used V genes in immune repertoires from patients with HA20 (Figs. 6A and 1D). The malignant clone showed a high IGHV mutation rate with identity to germline of around 81%. Sequencing of nonmalignant lymphocytes from the blood of patient HA20-14 showed a high level of B cell connectivity with IGHV3-23 making up the most frequently used BCR gene family in these nonmalignant lymphocyte networks (Fig. 6B).

Single-cell sequencing reveals lymphoma-like transcription signatures in lymphocytes of patients with HA20

On the basis of these data, we asked whether A20 loss not only favored proliferation of lymphocytes with permissive antigen receptors but also shifted global gene expression toward a lymphoma-like transcriptome. To test this hypothesis, we performed paired scRNA-seq and scBCR/TCR-seq of peripheral blood mononuclear cells (PBMCs) from two patients with HA20 (HA20-1 and HA20-21, 7691 cells) and one healthy donor (HD, 4741 cells) as well as a case of DLBCL with somatic A20 deficiency (3457 cells) (Fig. 6, C to J). Integration of the PBMC datasets revealed that patients with HA20 were characterized by the expansion of classical $CD14^+CD16^-$ and nonclassical monocytes $CD14^+CD16^+$ (17% of all HA20 cells versus <1% of all HD cells) as well as B cells (8 versus 2%) (Fig. 6C). In contrast, natural killer cells (12 versus 25%) and the T cell compartment (59 versus 69%) were contracted in patients with HA20 (Fig. 6C). Within the T cell population, a regulatory T cell (T_{reg})–like cluster (*CD4*, *FOXP3*, and *CTLA4*) was reduced in HA20 (25 versus 12%), while a memory-/effector-like population (*CD8A*, *CD27*, and *GZMK*) was expanded (13 versus 5%) (Fig. 6C). B cells from patients with HA20 had higher expression of NF-κB regulators or target genes associated with proliferation and lymphomagenesis (*FOXO1*, *BACH2*, *CD40*, *NEAT1*, *TNFRSF14*, and *KLF3*) (Fig. 6D). HA20 cells had on average a higher score for chronic inflammation [Gene Ontology (GO) term: GO0002544] as compared to B cells from HDs (Fig. 6E). In addition, HA20 B cells were characterized by a higher CD81/CD82 tetraspanin and JAK-STAT score (Fig. 6E). They shared these features with the expanded $CD8^+$ memory-/effector-like population (Fig. 6E). Within the T cell compartment, the HA20 T_{reg}-like cluster displayed higher expression of *TOX*, *PDCD1*, and *TIGIT* indicative of chronic activation and exhaustion (Fig. 6F). The same factors in addition to *LAG3* and *EOMES* were also highly expressed in the effector-like $CD8^+/\gamma\delta$ T cell compartment and naïve-like $CD4^+$ T cells (Fig. 6E). The latter also showed increased expression of *GATA3*, a master transcription factor for T_H2 polarization.

We compared these A20 haploinsufficient cells with lymph node material of an A20-deficient DLBCL. This case revealed two *TNFAIP3*-deficient lymphoma B cell subpopulations classified by expression of markers for germinal center commitment (*MEF2B* and *TCF4*) or plasma cell differentiation (*PRDM1* and *JCHAIN*) (Fig. 6G) and the presence of different CD4 T_{regs} and central memory cells, as well as activated and cytotoxic T cells as predominant bystander populations (Fig. 6G). To visualize the potential developmental trajectory from healthy to HA20-derived lymphocytes to lymphoma cells, we integrated all CD20 and/or CD19 expressing B cells from the three datasets and subjected them to potential of heat diffusion for affinity-based trajectory embedding (PHATE) analysis (Fig. 6H). This analysis revealed HA20 B cells as intermediate population between healthy and fully transformed lymphoma B cells (Fig. 6H). Analysis of all up- or down-regulated genes within the trajectory showed up-regulations of *CD81* and *MAP2K2*, while *CD19*, *MS4A1*, and *BIRC3* were down-regulated along the trajectory (Fig. 6I). Pathway enrichment analysis suggested substantial enrichment of genes linked to TNF-mediated signaling, the ubiquitin-proteasome machinery and apoptosis along the trajectory from healthy B cells to lymphoma (Fig. 6J).

DISCUSSION

In this work, we demonstrate that A20, an inhibitor of NF-κB constituting one of the important signaling cascades downstream antigen receptors, is capable of regulating the architectural shape of immune repertoires by preventing the outgrowth of distinct permissive lymphocyte sets poised for malignant transformation. We gained this unprecedented insight into the very early steps of lymphomagenesis by analyzing a cohort of patients with the HA20 syndrome who carry germline A20 mutations of identical functionality as the somatic A20 mutations found in lymphomas. In contrast to genetically engineered animal or lymphoma models, the analysis of immune repertoires of individuals with HA20 provides a window into veritable long-term effects and consequences of these mutations on human nonmalignant lymphocytes under conditions of natural clonal competition.

Although the A20-NF-κB axis is crucial for lymphoma development (*10*, *11*, *13*, *14*, *17*, *30*, *31*), its dysregulation is not sufficient to mediate BCR-independent B cell survival (*32*, *33*). Consistent with that, *TNFAIP3*-mutant B cell lymphomas display a disproportionately high co-occurrence with oncogenic *MYD88* mutations that synergize with NF-κB activation but also trigger JAK-STAT signaling (*17*, *34*–*36*). This was also the case in one of our patients with HA20 who developed lymphoma after acquisition of a second A20 mutation and an *MYD88* mutation. In light of our data, it is plausible to assume that patients with HA20 are at increased lymphoma risk, and clinically unrecognized HA20 in some lymphoma cases reported in the literature further supports this notion (*37*). TNF antagonism may therefore be appropriate for symptom control in HA20 but may also ensure homeostasis of adaptive immune repertoires and prevent lymphomagenesis. Because of the limited access to more patients with HA20, we could not confirm these findings in more patients. However, there is an increasing number of HA20 case reports that show no response to a range of immunosuppressive treatment approaches but solid responses to TNF blockade as observed in our case (*38*–*41*). While this observation is no definitive proxy for the exact same immune repertoire dynamics pre- and post-treatment, it emphasizes the key role of TNF in a substantial proportion of patients with HA20 in line with the here proposed model. Of note, the antiproliferative effect of TNF antagonism in our established lymphoma cell lines was consistent across experiments but small. This supported our hypothesis that A20 mutations—through auto- or paracrine TNF—may support the initial steps of lymphomagenesis in that they impede the censoring of self-reactive lymphocytes carrying permissive antigen receptors. These TNF-mediated mechanisms are likely not as important for established lymphomas that have undergone a complex multistep mutational process creating tumor drivers that confer more independence from environmental inflammatory stimuli.

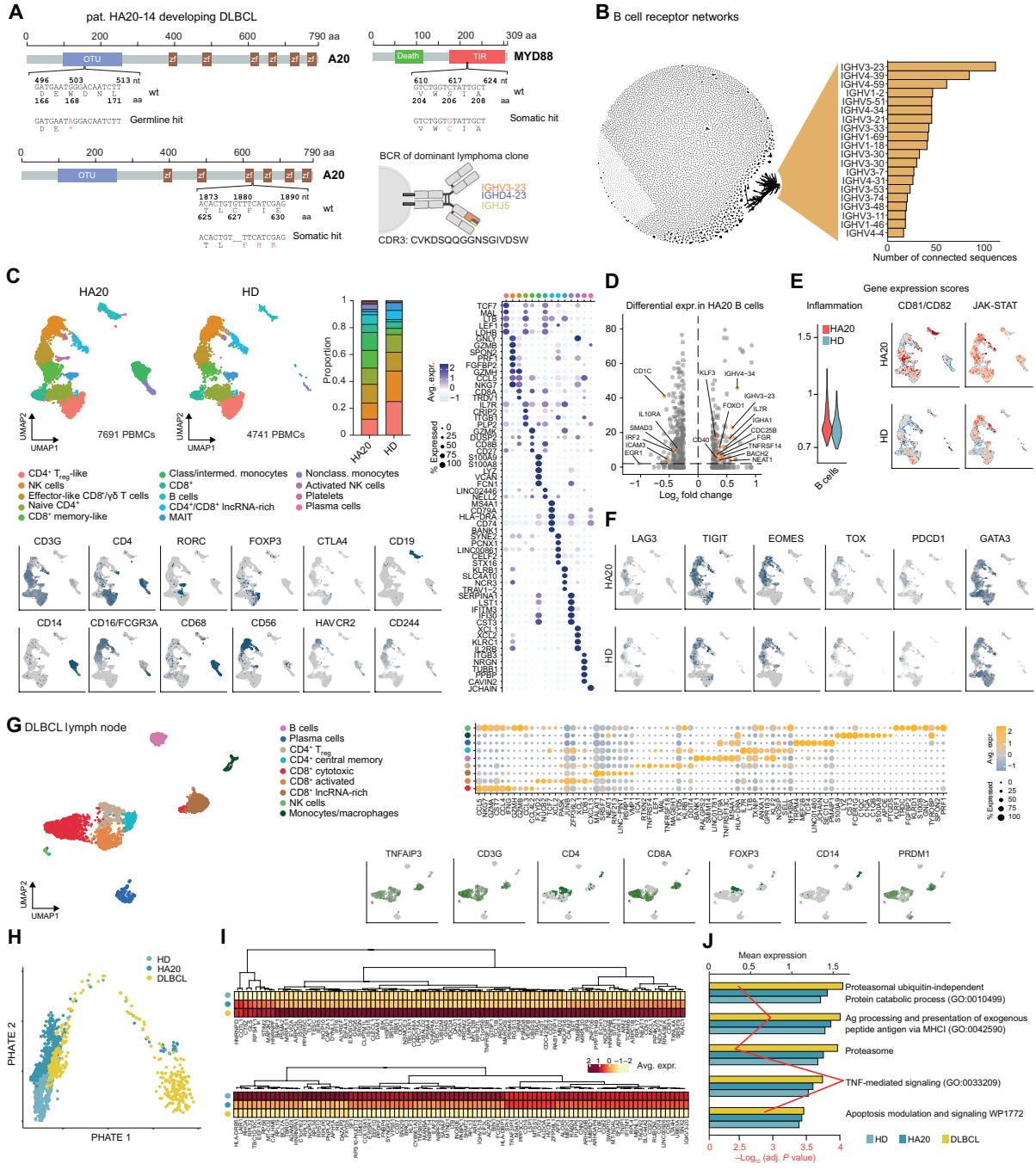

Fig. 6. Genomic and transcriptional signatures of HA20 suggest continuous trajectories toward lymphoma development. (**A**) Gene panel analysis of patient HA20-14 who developed DLBCL after acquiring additional *TNFAIP3* and *MYD88* mutations. The BCR configuration of the malignant clone is indicated. nt, nucleotide; aa, amino acid; OTU, ovarian tumor protease deubiquitinase domain; zf, zinc finger; Death, Death domain; TIR, Toll/IL-1 receptor interacting domain; CDR3, Complementarity-determining region 3. (**B**) Connectivity analysis of nonmalignant peripheral B cell clones in the repertoire of patient HA20-14. Clones with Levenshtein distance ≤3 are considered connected. The numbers of connected IGHV gene sequences of the persisting network are shown as bars. (**C**) UMAP of integrated PBMC dataset from two patients with HA20 (HA20-1: 1454 cells; HA20-34: 6237 cells) and one HD (4741 cells). Cluster proportion as stacked bar plots. Top five differentially expressed genes per cluster as dot plots and expression of signature genes for cluster definition as feature plots. (**D**) Volcano plot showing differentially expressed genes between healthy and HA20 B cells. Only differences with adjusted $P < 0.01$ were considered relevant. (**E**) Expression score for indicated processes/pathways. (**F**) Chronic activation/exhaustion markers in HA20 and HD T cell subsets. (**G**) UMAP projection of 3457 single lymph node cells from an A20-deficient patient with ABC DLBCL. The top 10 differentially expressed genes per cluster are shown as dot plot and expression of key signature genes for identification of immune cell subsets as feature plot. (**H**) PHATE mapping revealed HA20 B cells (dark cyan) as intermediate group between healthy (light cyan) and ABC DLBCL B cells (yellow). (**I**) Heatmap showing the top 100 monotonically increasing or decreasing genes within the HD-HA20-ABC DLBCL trajectory. (**J**) Enrichment of GO Terms displayed as mean expression levels per group (upper axis). Red line and corresponding lower *x* axis indicate $-\log_{10}$ adjusted *P* values of enriched terms.

The increased risk for lymphoma is also conceivable from the broad transcriptional changes in peripheral HA20 immune cells. The PHATE analysis identified HA20 B cells as an intermediate population between healthy B cells and lymphoma cells that are characterized by activation of TNF and JAK-STAT signaling as well as CD81 and CD82 up-regulation required for BCR nanocluster organization that mediates tonic or enhanced BCR signaling (*42*–*44*). Their up-regulation might contribute to the formation of oligomeric BCR clusters that mimic chronic antigen-dependent BCR ligation and are often found on the plasma membranes of lymphoma (*33*, *45*). Notably, this hypothesis is based on a small cohort and needs further validation. In the HA20 T lineage, we found transcriptional signatures reminiscent of T cell lymphomas, including characteristic up-regulation of markers of chronic activation and exhaustion as well as JAK-STAT, *CD82*, and *GATA3* (*46*–*48*). These cross-lineage patterns emphasize their relevance as general lymphoma drivers with therapeutic potential (*46*, *49*).

Unexpectedly, our animal model with monocyte/macrophage-specific A20 deletion showed that excessive TNF alone might induce selective proliferative effects in (especially T) lymphocytes even if the lymphocytes themselves are A20 proficient. Therefore, the relevance of TNF for lymphomagenesis may have broader clinical implications. There is a growing body of evidence supporting the role for myeloid-derived cytokines in support of lymphoid malignancies. In addition, gastric mucosa-associated lymphoid tissue (MALT) lymphoma may be an example that supports the importance of cytokines. While *Helicobacter pylori*–dependent cases may achieve remission by eradication of the inflammatory stimulus, *H. pylori*–independent cases often activate the NF-κB pathway by oncogenic products of specific chromosomal translocations such as t(11;18)/API2-MALT1 or inactivation of A20 that may mimic the inflammatory microenvironment induced by Helicobacter.

Another intriguing aspect of our work relates to the very specific antigen receptor configurations forming a proliferative interactome with *TNFAIP3* LOF mutations. Most prominently, TRBV20-1 pairings have been found in expanded T cell clones from patients with HA20. TRBV20-1 is frequently used in autoreactive T cell repertoires directed against self-antigens (*50*, *51*). Likewise, in autoimmune hepatitis—a disease with high TNF levels that is driven by autoreactive CD4 T cells and increased risk of lymphoma—our group has previously observed increased usage of TRBV20-1 by T cells (*52*, *53*). In T cell lymphomas, we found TRBV20-1 to be strongly associated with *TNFAIP3* LOF. Two examples of BCRs associated with *TNFAIP3* LOF mutations are IGHV4-34, which conveys reactivity with conserved carbohydrate self-epitopes and commensal bacteria (*54*, *55*), and IGHV3-7, which has been shown to react with apoptotic material (*33*). Taking IGHV4-34 as an example, we were able to demonstrate that even healthy B cells using this class of receptors tend to down-regulate A20, therefore signaling preferentially via NF-κB. This convergence on the same signaling pathway may be the reason why *TNFAIP3* LOF mutations expand lymphocytes with antigen receptor configurations preferentially engaging NF-κB.

Together, our work demonstrates that A20 can regulate immune repertoire homeostasis by restricting the expansion of distinct lymphocytes with permissive antigen receptor configurations. We provide evidence for broad transcriptional changes toward lymphoma-like signatures after heterozygous loss of *TNFAIP3*, suggesting an elevated lymphoma risk in patients with HA20. In this way, HA20 provides important insights into the protracted pre-malignant phases of lymphocyte selection that remain clinically unrecognized. Dissecting these early phases of lymphomagenesis could affect innovative programs of early detection, early treatment, and even prevention.

MATERIALS AND METHODS

Patients and samples

Peripheral blood of patients with germline *TNFAIP3* mutations (in patient HA20-1 before and after treatment initiation) and 36 healthy control individuals was collected for scientific purposes after informed consent as approved by the ethics commission Halle (Saale) (project number 2014-75). Functional information of already published *TNFAIP3* mutations from HA20 families can be obtained from the Infevers database (*56*) (https://infevers.umai-montpellier.fr/). All patients with HA20 gave written informed consent. The protocol was approved by the National Human Genome Research Institute (NHGRI) Institutional Review Board. Paraffin-embedded lymphoma tissue of a cohort of 51 patients with ABC-type DLBCL were collected as anonymized samples. The study has been performed in accordance with the Declaration of Helsinki of 1975.

Isolation of genomic DNA

PBMCs were isolated from peripheral blood by density-gradient centrifugation using Biocoll separation solution (Biochrom AG, Berlin, Germany). Genomic DNA of PBMCs and lymphoma tissue was isolated using the GenElute mammalian genomic DNA miniprep kit (Sigma-Aldrich, Taufkirchen, Germany) according to the manufacturer's instructions.

Amplification of IGH and TRB repertoire for NGS

The rearranged V, D, and J gene segments of the human IGH (IGHV, IGHD, and IGHJ) and TRB (TRBV, TRBD, and TRBJ) loci were amplified in a multiplex polymerase chain reaction (PCR) using BIOMED2-FR1 (IGH) or -TRB-B primer pools together and 250 ng of genomic DNA. The murine TRB primer set was derived from (*57*); murine IGH primers are listed in table S3. The primers were purchased from Metabion International AG (Martinsried, Germany). As described in (*58*), two consecutive PCR reactions were performed to generate IGH and TRB fragments tagged with Illumina-compatible adapters for hybridization to the flow cell and seven nucleotide barcodes for sample identification. All PCRs were performed using Phusion HS II (Thermo Fisher Scientific Inc., Darmstadt, Germany). After gelelectrophoretic separation, IGH and TRB amplicons were purified using the NucleoSpin Gel and PCR Clean-up kit (Macherey-Nagel, Düren, Germany), quantified on the Qubit platform (QIAGEN, Hilden, Germany), and pooled to a final concentration of 8 nM. The quality of the IGH and TRB amplicon pools was controlled on an Agilent 2100 Bioanalyzer (Agilent Technologies, Böblingen, Germany) before being subjected to NGS.

Immune repertoire NGS and data analysis

NGS and demultiplexing were performed on an Illumina MiSeq sequencer (600-cycle single-indexed, paired-end run, V3-chemistry). Analysis of the rearranged IGH and TRB loci was computed using the MiXCR framework (*59*). As reference for sequence alignment, the default MiXCR library was used for TRB sequences and the IMGT library v3 for IGH. Nonproductive reads and sequences with less than two read counts were not considered for further bioinformatics evaluation. All human repertoires were normalized to 20,000 and all murine repertoires to 30,000 reads. Each unique complementarity-determining

region 3 (CDR3) nucleotide sequence was considered a clone. All analyses and data plotting was performed using RStudio (version 1.1.456) and the tcR (*60*), ade4 (*61*), and tidyverse (*62*) packages.

Immune repertoire metrics

We calculated the clonality of the sequenced IGH and TRB repertoires according to the formula "1- Pielou's evenness" (*63*). In our setting, evenness measures the relative abundance of unique B or T cell clones in the repertoire and is calculated according to the formula $J = H'/\log_2(S)$ with H' being the Shannon diversity index and S the total clone number in a distinct sample (*64*). A clonality index of 1 indicates that the analyzed sample contains only one clone, whereas 0 indicates complete clonal diversity. IGHV genes with ≤98% identity to the germline sequence were considered antigen-experienced.

Gene panel NGS

For mutational profiling of lymphoma DNA, 100 ng of tumor FFPE tissue DNA were used. Target genes (*TNFAIP3*, *MYD88*, *CARD11*, *CD79B*, *CREBBP*, *EP300*, *IRF4*, *PIM1*, *TP53*, *TCF3*, *PRDM1*, *TRAF2*, *TRAF5*, *MYC*, *MEF2B*, *B2M*, *MAP3K7*, *TNFRSF11A*, and *ID3*) were selected on the basis of their frequency in ABC DLBCL through a review of published literature and by using the cBio Cancer Genomics Portal (*65*). Either the entire coding region or hotspot regions containing known pathogenic variants were targeted, and sequencing libraries were constructed using QIAseq Targeted DNA Custom Panels (Qiagen). Quantification and quality control of libraries was conducted using Qubit high-sensitivity double-strand DNA assay kit (Thermo Fisher Scientific) and Agilent 2100 Bioanalyzer (Agilent). Sequencing was performed on the Illumina NextSeq or HiSeq platform with 2 × 151 cycles at an average coverage of 26,500 reads per target region. Variant calling of unique molecular identifier–based sequencing data was performed using smCounter2 as described elsewhere (*66*).

Analysis of whole-exome sequencing data

Whole-exome sequencing data of cutaneous T cell non-Hodgkin lymphoma MF/SS were downloaded from the National Institutes of Health database of Genotypes and Phenotypes (dbGaP; accession number phs000859). For our analyses, we used 27 of the 33 deposited BAM files with sufficient read depth for TRBV gene assignment and *TNFAIP3* mutation calling. To assign TRBV genes, we cut the corresponding regions using samtools (*67*) function view followed by germline alignment using Igblast (*68*). For *TNFAIP3* mutation calling, BAM files were trimmed down to the respective gene regions using samtools function view and by applying gatk (v4.1.9.0, broadinstitute.org) functions mutect2 and FilterMutectCalls. Resulting vcf-files were annotated with Annovar (*69*).

Cytokine profiling

Plasma was isolated by centrifugation of whole blood for 15 min at 2000*g*. Samples were stored at −80°C before use. Cytokine plasma levels were measured as duplicates using the LEGENDplex Human B Cell Panel (13-plex) and the LEGENDplex Mouse B cell Panel (13-plex; BioLegend via Biozol, Munich, Germany) according to the supplier's suggestions. To assess cytokine secretion of lymphoma cell lines, 1×10^6 cells were seeded and supernatants were harvested after 72 hours of incubation. For inhibition or activation of NF-κB, 2×10^6 cells were seeded in six-well plates and incubated with 100 μM PDTC ammonium (Selleckchem) or recombinant TNF (100 ng/ml, Sigma-Aldrich) for 1 hour. Data were acquired using the BD FACSCelesta or CytoFLEX flow cytometers and analyzed with the BioLegend LEGENDplex software. In case of TNF, obtained levels were normalized to culture medium supplemented with TNF (100 ng/ml).

Antibodies and cell lines

The following antibodies were used for immunoblotting: anti-A20 (clone D13H3) and anti–TATA box–binding protein (TBP) from Cell Signaling technology (Heidelberg, Germany); anti-p65 (F-6), anti–glyceraldehyde-3-phosphate dehydrogenase (6C5), and anti–β-actin (C4) from Santa Cruz Biotechnology (Heidelberg, Germany). Horseradish peroxidase (HRP)–linked anti-rabbit IgG (HAF008) and HRP-linked anti-mouse IgG (HAF007) were purchased from R&D Systems (Minneapolis, United States). The human embryonal kidney cell line 293T and the human B cell lymphoma cell lines OCI-Ly3 and RI-1 were obtained from DSMZ (Braunschweig, Germany). The lymphoma lines were cultured in RPMI 1640 supplemented with 10% (v/v) fetal calf serum (FCS, RI-1) or 20% FCS (OCI-Ly3), the 293T cell lines in Dulbecco's modified Eagle's medium supplemented with 10% FCS. The 293T, OCI-Ly3, and RI-1 cell lines were supplemented with 1% (v/v) penicillin-streptomycin and incubated at 37°C and 5% CO_2. Phoenix-eco and TKO cells were cultured in Iscove's modified Dulbecco's medium (Sigma-Aldrich, I3390-500ML) with 10 and 5% FCS (Life Technologies GmbH, 10500064), respectively, and were supplemented with penicillin-streptomycin (100 U/ml, Thermo Fisher Scientific, 15140122), 2 mM L-glutamine (Thermo Fisher Scientific, 25030024), and 50 μM β-ME (Thermo Fisher Scientific, 31350010). TKO medium was further supplemented with recombinant human IL-7 (1 ng/ml, Peprotech 200-07, cross-reactive with mouse). Phoenix-eco and TKO cells were incubated at 37°C and 7.5% CO_2.

Expression constructs and Lenti- or retroviral transduction

For A20 overexpression, the cDNA of *TNFAIP3* was isolated from OCI-Ly3 via reverse transcription (SuperScript III, Thermo Fisher Scientific) of total RNA and cloned into the Lentiviral Gene Ontology (LeGO) vector LeGO-iC2-Puro+ via *Asi*SI and *Eco*RI (*70*). Viral particles were generated in 293T cells with the third-generation packaging plasmids pMDLg/pRRE and pRSV-Rev and used for transduction of 5×10^4 target cells in the presence of polybrene (8 μg/ml) while centrifuging 1 hour at 1000*g* as described in (*70*). Successfully transduced target cells were selected with puromycin (100 μg/ml).

For expression of selected BCRs, patient-derived BCR heavy chain (HC) and light chain (LC) sequences (table S4) were synthesized via GeneArt (Thermo Fisher Scientific). BCR HCs encompassed the complete rearranged VDJ sequence but lacked the constant region. HCs were cloned in-frame to the adjacent murine μ constant chain in the pMIZCC vector via *Xho*I and *Psh*AI. LCs encompassed their respective kappa or lambda constant region and were cloned into pMIZYN via *Xho*I and *Eco*RI. All constructs were generated using the In-Fusion cloning system (Takara, Heidelberg) according to the manufacturer's instructions.

For production of viral supernatant, Phoenix-eco cells were seeded at $0.5 * 10^6$ cells per well in six-well plates 24 hours before transfection. For transfection, a total of 1 μg of DNA was used alongside 3 μg of PEI MAX (Polysciences 24765-100) per well. DNA mix consisted of one-third each of a plasmid containing the LC sequence (variable and constant region, both human), the HC sequence (human variable region fused to murine μ constant region), and the pKAT packaging plasmid to increase virus production.

Viral supernatant was collected after 48 hours incubation at 37°C, filtered through a 0.45-μm filter, and concentrated using Lenti-X Concentrator (Clontech 631231) overnight. Transductions were performed by resuspending 2.5 ∗ 10^5 TKO cells within 2.0-ml tubes in TKO medium containing polybrene (10 μg/ml, Merck Millipore TR-1003-G) and freshly produced and concentrated viral supernatant followed by spinoculation for 3 hours at 37°C and 300*g*.

Immunoblotting

For monitoring the A20 status, whole cell extracts from cell lines were generated using radioimmunoprecipitation assay buffer (Thermo Fisher Scientific) supplemented with protease and phosphatase inhibitors (Roche, Basel, Switzerland). Constitutive or induced NF-κB activation was assessed by monitoring nuclear translocation of p65 via immunoblotting. Cytoplasmic and nuclear extracts were generated with the Nuclear Extract Kit (Active Motif, La Hulpe, Belgium). Proteins were quantified using Bradford. After separation of 20 to 30 μg extracts on 10% NuPAGE Bis-Tris gels (Thermo Fisher Scientific) under denaturing conditions, proteins were blotted under semi-dry conditions.

Proliferation assays

For proliferation of lymphoma cell lines, cells were seeded at 1 × 10^6 cells/ml and treated with infliximab (100 ng/ml), human IgG (100 ng/ml, Intratect, BIOTEST Pharma GmbH), or left untreated. After 72 hours, viable cells were quantified by trypan blue staining using the Cell Viability Analyzer Vi-Cell XR (Beckman Coulter).

RNA sequencing

Total RNA was isolated using the Quick-RNA kit (Zymo Research) and reverse transcribed with SuperScript III (Thermo Fisher Scientific). RNA integrity and quantitation were performed using the Bioanalyzer 2100 system (Agilent Technologies). Library preparation and sequencing was performed by Novogene as service. Raw reads were mapped to the human genome (gencode.v29) with STAR (v.2.7.3a) and the read counts processed using package DESeq2 (v.1.34) (*71*) in Rstudio (R version 4.1.2). After normalization, differential expression analysis was performed with function lfcShrink and type "ashr" (*72*). Genes were annotated using package biomart (*73*). Pathway analysis was done with package enrichR (*74*), and volcano plot was visualized using package EnhancedVolcano.

Calcium signaling

For calcium flux measurements, 1.5 million TKO cells were loaded with Indo-1 AM (Thermo Fisher Scientific, I1223) using Pluronic F-127 (Invitrogen, P3000MP) and stimulated with either 2 μM 4-hydroxytamoxifen (4-OHT, Merck, H7904) for measuring of autonomous signaling capabilities by induction of SLP65-ERT2 or 2 μM 4-OHT + 10 μg/ml anti-IgM (Sigma-Aldrich AP500 Goat Anti-Mouse IgM) for BCR cross-linking. As loading control to achieve maximum cytosolic calcium levels, Ionomycin (4 μg/ml, Stem Cell Technology, 73722) were added. All measurements were performed at 37°C using a custom three-dimensionally (3D)–printed tube holder connected to a water pump and heating unit on a BD LSR Fortessa flow cytometer.

Experimental model and subject details

All mice were on the C57BL/6J background and were housed under specific pathogen–free conditions. $A20^{fl/fl}$ mice were bred to Cx3cr1-$Cre^{ERT2/+}$ (*28*, *29*) or CD19-Cre mice (*6*) performed in accordance with the guidelines from the Central Animal Facility Institution at the Johannes-Gutenberg University Mainz, Germany. For induction of Cre recombinase in $A20^{fl/fl}$Cx3cr1-$Cre^{ERT2/+}$ ($A20^{Cx3cr1\text{-}KO}$), a 20 mg/ml solution of tamoxifen (Sigma-Aldrich) was prepared by suspension in olive oil (Sigma-Aldrich) at 37°C for 2 hours on a shaker. Pups were injected subcutaneously with 2 mg of tamoxifen at postnatal day 14 (P14) and P16. PBMCs, thymus, spleen, (mesenteric) lymph nodes, and plasma were isolated from $A20^{Cx3cr1\text{-}KO}$ and $A20^{fl/fl}$CD19-Cre ($A20^{CD19\text{-}KO}$) mice at 4 weeks of age. For isolation, the mice were anesthetized by inhalation with isoflurane.

For TNF blockade, the mice were injected intraperitoneally with 100 μg of the InVivoPlus anti-mouse TNFα antibody (clone XT3.11) (BioXCell via Biozol, Echnig, Germany). The first injection was performed on the same day as the first tamoxifen injection (P14) and then every third day with the last injection on day 12.

Single-cell sequencing

scRNA-seq was performed as described in (*75*) using either PBMCs or FACS-sorted $CD19^+$ B cells that expressed IGHV4-34–encoded antigen receptors or non–IGHV4-34 antigen receptors. IGHV4-34 BCRs were enriched using the anti–IGHV4-34 antibody clone 9 g4 (IgmBiosciences, Mountain View, California, USA). Single-cell libraries were generated using the Chromium Next GEM Single Cell 5' Kit v2, Human BCR Amplification, and Human TCR Amplification kits (10X Genomics) as described in (*75*). Fastq files were processed to read counts with cellranger 5.0.1 software (10x Genomics), which includes alignment, filtering, and barcode counting. Read counts were loaded into Rstudio with Seurat (*76*) and a Seurat object was created. An integrated dataset of HA20-1, HA20-21, a DLBCL sample, and 23 published healthy individuals (*77*) was generated using Harmony (*78*) with the following procedure: Raw read matrices were concatenated to one big data matrix. An integrated object was created, normalized, and scaled. PCA was performed on the scaled data (function RunPCA, npcs = 20, features = NULL). Cells were reclustered with harmony and plotted as UMAP using Seurat on harmony embeddings. Gene expression scores were calculated using Seurat function AddModuleScore (nbin = 24 and ctrl = 100). Subsequently, a subset of all B cells was selected where we downsampled the HD group to 600 cells. For 2D data visualization, we performed PHATE (*78*, *79*) with kernel_symm = mutual nearest neighbors. To find monotonically increasing and decreasing genes between groups, we calculated the mean expression for each gene and group and then selected all genes that had an expression pattern healthy<HA20<DLBCL for increasing genes and vice versa for decreasing genes. Statistical significance was tested with Wilcoxon rank sum test. Heatmaps were created with package pheatmap. Enrichment analysis was performed with package enrichR on databases "KEGG_2019_Human," "GO_Molecular_Function_2018", "GO_Biological_Process_2018," and "WikiPathways_2019_Human" (*80*). Only GO terms with an adjusted *P* value lower than 0.01 were considered for further analysis. From selected GO terms, mean expression of corresponding genes per group were plotted with ggplot2. All Analysis steps were done using RStudio and R version 4.2.0.

Statistical analysis

Differences in NGS metrics and cytokine levels were studied by Student's *t* test or one-way analysis of variance (ANOVA). Differences in TNFAIP3 expression in scRNA-seq was determined using Mann-Whitney *U* test. All statistical analyses for cytokines were performed

with GraphPad Prism 8.0.2 (GraphPad Software, La Jolla, CA, USA) and the rest using RStudio and R version 4.2.0.

Supplementary Materials

This PDF file includes:

Figs. S1 and S2
Tables S1 to S3

REFERENCES AND NOTES

1. Q. Zhou, H. Wang, D. M. Schwartz, M. Stoffels, Y. H. Park, Y. Zhang, D. Yang, E. Demirkaya, M. Takeuchi, W. L. Tsai, J. J. Lyons, X. Yu, C. Ouyang, C. Chen, D. T. Chin, K. Zaal, S. C. Chandrasekharappa, E. P. Hanson, Z. Yu, J. C. Mullikin, S. A. Hasni, I. E. Wertz, A. K. Ombrello, D. L. Stone, P. Hoffmann, A. Jones, B. K. Barham, H. L. Leavis, A. van Royen-Kerkof, C. Sibley, E. D. Batu, A. Gul, R. M. Siegel, M. Boehm, J. D. Milner, S. Ozen, M. Gadina, J. Chae, R. M. Laxer, D. L. Kastner, I. Aksentijevich, Loss-of-function mutations in TNFAIP3 leading to A20 haploinsufficiency cause an early-onset autoinflammatory disease. *Nat. Genet.* **48**, 67–73 (2016).
2. I. Aksentijevich, Q. Zhou, NF-κB pathway in autoinflammatory diseases: Dysregulation of protein modifications by ubiquitin defines a new category of autoinflammatory diseases. *Front. Immunol.* **8**, 399 (2017).
3. T. Das, Z. Chen, R. W. Hendriks, M. Kool, A20/tumor necrosis factor α-induced protein 3 in immune cells controls development of autoinflammation and autoimmunity: Lessons from mouse models. *Front. Immunol.* **9**, 104 (2018).
4. S. G. Hymowitz, I. E. Wertz, A20: From ubiquitin editing to tumour suppression. *Nat. Rev. Cancer* **10**, 332–341 (2010).
5. R. M. Tavares, E. E. Turer, C. L. Liu, R. Advincula, P. Scapini, L. Rhee, J. Barrera, C. A. Lowell, P. J. Utz, B. A. Malynn, A. Ma, The ubiquitin modifying enzyme A20 restricts B cell survival and prevents autoimmunity. *Immunity* **33**, 181–191 (2010).
6. N. Hovelmeyer, S. Reissig, N. T. Xuan, P. Adams-Quack, D. Lukas, A. Nikolaev, D. Schluter, A. Waisman, A20 deficiency in B cells enhances B-cell proliferation and results in the development of autoantibodies. *Eur. J. Immunol.* **41**, 595–601 (2011).
7. A. Martens, G. van Loo, A20 at the crossroads of cell death, inflammation, and autoimmunity. *Cold Spring Harb. Perspect. Biol.* **12**, a036418 (2020).
8. K. Ishigaki, S. Sakaue, C. Terao, Y. Luo, K. Sonehara, K. Yamaguchi, T. Amariuta, C. L. Too, V. A. Laufer, I. C. Scott, S. Viatte, M. Takahashi, K. Ohmura, A. Murasawa, M. Hashimoto, H. Ito, M. Hammoudeh, S. A. Emadi, B. K. Masri, H. Halabi, H. Badsha, I. W. Uthman, X. Wu, L. Lin, T. Li, D. Plant, A. Barton, G. Orozco, S. M. M. Verstappen, J. Bowes, A. J. MacGregor, S. Honda, M. Koido, K. Tomizuka, Y. Kamatani, H. Tanaka, E. Tanaka, A. Suzuki, Y. Maeda, K. Yamamoto, S. Miyawaki, G. Xie, J. Zhang, C. I. Amos, E. Keystone, G. Wolbink, I. van der Horst-Bruinsma, J. Cui, K. P. Liao, R. J. Carroll, H. S. Lee, S. Y. Bang, K. A. Siminovitch, N. de Vries, L. Alfredsson, S. Rantapaa-Dahlqvist, E. W. Karlson, S. C. Bae, R. P. Kimberly, J. C. Edberg, X. Mariette, T. Huizinga, P. Dieude, M. Schneider, M. Kerick, J. C. Denny, P. B. B. Japan, K. Matsuda, K. Matsuo, T. Mimori, F. Matsuda, K. Fujio, Y. Tanaka, A. Kumanogoh, M. Traylor, C. M. Lewis, S. Eyre, H. Xu, R. Saxena, T. Arayssi, Y. Kochi, K. Ikari, M. Harigai, P. K. Gregersen, K. Yamamoto, S. Louis Bridges Jr., L. Padyukov, J. Martin, L. Klareskog, Y. Okada, S. Raychaudhuri, Multi-ancestry genome-wide association analyses identify novel genetic mechanisms in rheumatoid arthritis. *Nat. Genet.* **54**, 1640–1651 (2022).
9. B. Khatri, K. L. Tessneer, A. Rasmussen, F. Aghakhanian, T. R. Reksten, A. Adler, I. Alevizos, J. M. Anaya, L. A. Aqrawi, E. Baecklund, J. G. Brun, S. M. Bucher, M. L. Eloranta, F. Engelke, H. Forsblad-d'Elia, S. B. Glenn, D. Hammenfors, J. Imgenberg-Kreuz, J. L. Jensen, S. J. A. Johnsen, M. V. Jonsson, M. Kvarnstrom, J. A. Kelly, H. Li, T. Mandl, J. Martin, G. Nocturne, K. B. Norheim, O. Palm, K. Skarstein, A. M. Stolarczyk, K. E. Taylor, M. Teruel, E. Theander, S. Venuturupalli, D. J. Wallace, K. M. Grundahl, K. S. Hefner, L. Radfar, D. M. Lewis, D. U. Stone, C. E. Kaufman, M. T. Brennan, J. M. Guthridge, J. A. James, R. H. Scofield, P. M. Gaffney, L. A. Criswell, R. Jonsson, P. Eriksson, S. J. Bowman, R. Omdal, L. Ronnblom, B. Warner, M. Rischmueller, T. Witte, A. D. Farris, X. Mariette, M. E. Alarcon-Riquelme; PRECISEADS Clinical Consortium, C. H. Shiboski; Sjögren's International Collaborative Clinical Alliance (SICCA), M. Wahren-Herlenius, W. F. Ng; UK Primary Sjögren's Syndrome Registry, K. L. Sivils, I. Adrianto, G. Nordmark, C. J. Lessard, Genome-wide association study identifies Sjogren's risk loci with functional implications in immune and glandular cells. *Nat. Commun.* **13**, 4287 (2022).
10. M. Compagno, W. K. Lim, A. Grunn, S. V. Nandula, M. Brahmachary, Q. Shen, F. Bertoni, M. Ponzoni, M. Scandurra, A. Califano, G. Bhagat, A. Chadburn, R. Dalla-Favera, L. Pasqualucci, Mutations of multiple genes cause deregulation of NF-κB in diffuse large B-cell lymphoma. *Nature* **459**, 717–721 (2009).
11. M. Kato, M. Sanada, I. Kato, Y. Sato, J. Takita, K. Takeuchi, A. Niwa, Y. Chen, K. Nakazaki, J. Nomoto, Y. Asakura, S. Muto, A. Tamura, M. Iio, Y. Akatsuka, Y. Hayashi, H. Mori, T. Igarashi, M. Kurokawa, S. Chiba, S. Mori, Y. Ishikawa, K. Okamoto, K. Tobinai, H. Nakagama, T. Nakahata, T. Yoshino, Y. Kobayashi, S. Ogawa, Frequent inactivation of A20 in B-cell lymphomas. *Nature* **459**, 712–716 (2009).
12. U. Novak, A. Rinaldi, I. Kwee, S. V. Nandula, P. M. Rancoita, M. Compagno, M. Cerri, D. Rossi, V. V. Murty, E. Zucca, G. Gaidano, R. Dalla-Favera, L. Pasqualucci, G. Bhagat, F. Bertoni, The NF-κB negative regulator *TNFAIP3* (A20) is inactivated by somatic mutations and genomic deletions in marginal zone lymphomas. *Blood* **113**, 4918–4921 (2009).
13. R. Schmitz, G. W. Wright, D. W. Huang, C. A. Johnson, J. D. Phelan, J. Q. Wang, S. Roulland, M. Kasbekar, R. M. Young, A. L. Shaffer, D. J. Hodson, W. Xiao, X. Yu, Y. Yang, H. Zhao, W. Xu, X. Liu, B. Zhou, W. Du, W. C. Chan, E. S. Jaffe, R. D. Gascoyne, J. M. Connors, E. Campo, A. Lopez-Guillermo, A. Rosenwald, G. Ott, J. Delabie, L. M. Rimsza, K. T. K. Wei, A. D. Zelenetz, J. P. Leonard, N. L. Bartlett, B. Tran, J. Shetty, Y. Zhao, D. R. Soppet, S. Pittaluga, W. H. Wilson, L. M. Staudt, Genetics and pathogenesis of diffuse large B-cell lymphoma. *N. Engl. J. Med.* **378**, 1396–1407 (2018).
14. L. Pasqualucci, R. Dalla-Favera, Genetics of diffuse large B-cell lymphoma. *Blood* **131**, 2307–2319 (2018).
15. F. C. Braun, P. Grabarczyk, M. Mobs, F. K. Braun, J. Eberle, M. Beyer, W. Sterry, F. Busse, J. Schroder, M. Delin, G. K. Przybylski, C. A. Schmidt, Tumor suppressor TNFAIP3 (A20) is frequently deleted in Sézary syndrome. *Leukemia* **25**, 1494–1501 (2011).
16. A. A. Ferrando, C. Lopez-Otin, Clonal evolution in leukemia. *Nat. Med.* **23**, 1135–1145 (2017).
17. A. L. Shaffer III, R. M. Young, L. M. Staudt, Pathogenesis of human B cell lymphomas. *Annu. Rev. Immunol.* **30**, 565–610 (2012).
18. M. Greaves, C. C. Maley, Clonal evolution in cancer. *Nature* **481**, 306–313 (2012).
19. S. Meixlsperger, F. Kohler, T. Wossning, M. Reppel, M. Muschen, H. Jumaa, Conventional light chains inhibit the autonomous signaling capacity of the B cell receptor. *Immunity* **26**, 323–333 (2007).
20. M. Duhren-von Minden, R. Ubelhart, D. Schneider, T. Wossning, M. P. Bach, M. Buchner, D. Hofmann, E. Surova, M. Follo, F. Kohler, H. Wardemann, K. Zirlik, H. Veelken, H. Jumaa, Chronic lymphocytic leukaemia is driven by antigen-independent cell-autonomous signalling. *Nature* **489**, 309–312 (2012).
21. R. A. Reyes, G. Batugedara, P. Dutta, A. B. Reers, R. Garza, I. Ssewanyana, P. Jagannathan, M. E. Feeney, B. Greenhouse, S. Bol, F. Ay, E. M. Bunnik, Atypical B cells consist of subsets with distinct functional profiles. *iScience* **26**, 108496 (2023).
22. H. J. Sutton, R. Aye, A. H. Idris, R. Vistein, E. Nduati, O. Kai, J. Mwacharo, X. Li, X. Gao, T. D. Andrews, M. Koutsakos, T. H. O. Nguyen, M. Nekrasov, P. Milburn, A. Eltahla, A. A. Berry, N. Kc, S. Chakravarty, B. K. L. Sim, A. K. Wheatley, S. J. Kent, S. L. Hoffman, K. E. Lyke, P. Bejon, F. Luciani, K. Kedzierska, R. A. Seder, F. M. Ndungu, I. A. Cockburn, Atypical B cells are part of an alternative lineage of B cells that participates in responses to vaccination and infection in humans. *Cell Rep.* **34**, 108684 (2021).
23. R. Yang, D. T. Avery, K. J. L. Jackson, M. Ogishi, I. Benhsaien, L. Du, X. Ye, J. Han, J. Rosain, J. N. Peel, M. A. Alyanakian, B. Neven, S. Winter, A. Puel, B. Boisson, K. J. Payne, M. Wong, A. J. Russell, Y. Mizoguchi, S. Okada, G. Uzel, C. C. Goodnow, S. Latour, J. El Bakkouri, A. Bousfiha, K. Preece, P. E. Gray, B. Keller, K. Warnatz, S. Boisson-Dupuis, L. Abel, Q. Pan-Hammarstrom, J. Bustamante, C. S. Ma, J. L. Casanova, S. G. Tangye, Human T-bet governs the generation of a distinct subset of CD11c^{high}CD21^{low} B cells. *Sci. Immunol.* **7**, eabq3277 (2022).
24. P. Holla, B. Dizon, A. A. Ambegaonkar, N. Rogel, E. Goldschmidt, A. K. Boddapati, H. Sohn, D. Sturdevant, J. W. Austin, L. Kardava, L. Yuesheng, P. Liu, S. Moir, S. K. Pierce, A. Madi, Shared transcriptional profiles of atypical B cells suggest common drivers of expansion and function in malaria, HIV, and autoimmunity. *Sci. Adv.* **7**, eabg8384 (2021).
25. S. F. Liu, X. Ye, A. B. Malik, Inhibition of NF-κB activation by pyrrolidine dithiocarbamate prevents in vivo expression of proinflammatory genes. *Circulation* **100**, 1330–1337 (1999).
26. M. Matmati, P. Jacques, J. Maelfait, E. Verheugen, M. Kool, M. Sze, L. Geboes, E. Louagie, C. Mc Guire, L. Vereecke, Y. Chu, L. Boon, S. Staelens, P. Matthys, B. N. Lambrecht, M. Schmidt-Supprian, M. Pasparakis, D. Elewaut, R. Beyaert, G. van Loo, A20 (TNFAIP3) deficiency in myeloid cells triggers erosive polyarthritis resembling rheumatoid arthritis. *Nat. Genet.* **43**, 908–912 (2011).
27. L. Vande Walle, N. Van Opdenbosch, P. Jacques, A. Fossoul, E. Verheugen, P. Vogel, R. Beyaert, D. Elewaut, T. D. Kanneganti, G. van Loo, M. Lamkanfi, Negative regulation of the NLRP3 inflammasome by A20 protects against arthritis. *Nature* **512**, 69–73 (2014).
28. S. Yona, K. W. Kim, Y. Wolf, A. Mildner, D. Varol, M. Breker, D. Strauss-Ayali, S. Viukov, M. Guilliams, A. Misharin, D. A. Hume, H. Perlman, B. Malissen, E. Zelzer, S. Jung, Fate mapping reveals origins and dynamics of monocytes and tissue macrophages under homeostasis. *Immunity* **38**, 79–91 (2013).
29. A. N. Mohebiany, N. S. Ramphal, K. Karram, G. Di Liberto, T. Novkovic, M. Klein, F. Marini, M. Kreutzfeldt, F. Hartner, S. M. Lacher, T. Bopp, T. Mittmann, D. Merkler, A. Waisman, Microglial A20 protects the brain from CD8 T-cell-mediated immunopathology. *Cell Rep.* **30**, 1585–1597.e6 (2020).
30. Y. Sasaki, K. Iwai, Roles of the NF-κB pathway in B-lymphocyte biology. *Curr. Top. Microbiol. Immunol.* **393**, 177–209 (2016).
31. M. Singh, K. J. L. Jackson, J. J. Wang, P. Schofield, M. A. Field, D. Koppstein, T. J. Peters, D. L. Burnett, S. Rizzetto, D. Nevoltris, E. Masle-Farquhar, M. L. Faulks, A. Russell, D. Gokal, A. Hanioka, K. Horikawa, A. D. Colella, T. K. Chataway, J. Blackburn, T. R. Mercer,

D. B. Langley, D. M. Goodall, R. Jefferis, M. Gangadharan Komala, A. D. Kelleher, D. Suan, M. Rischmueller, D. Christ, R. Brink, F. Luciani, T. P. Gordon, C. C. Goodnow, J. H. Reed, Lymphoma driver mutations in the pathogenic evolution of an iconic human autoantibody. *Cell* **180**, 878–894.e19 (2020).
32. D. R. Myers, J. Zikherman, J. P. Roose, Tonic signals: Why do lymphocytes bother? *Trends Immunol.* **38**, 844–857 (2017).
33. R. M. Young, T. Wu, R. Schmitz, M. Dawood, W. Xiao, J. D. Phelan, W. Xu, L. Menard, E. Meffre, W. C. Chan, E. S. Jaffe, R. D. Gascoyne, E. Campo, A. Rosenwald, G. Ott, J. Delabie, L. M. Rimsza, L. M. Staudt, Survival of human lymphoma cells requires B-cell receptor engagement by self-antigens. *Proc. Natl. Acad. Sci. U.S.A.* **112**, 13447–13454 (2015).
34. K. Wenzl, M. K. Manske, V. Sarangi, Y. W. Asmann, P. T. Greipp, H. R. Schoon, E. Braggio, M. J. Maurer, A. L. Feldman, T. E. Witzig, S. L. Slager, S. M. Ansell, J. R. Cerhan, A. J. Novak, Loss of TNFAIP3 enhances MYD88L265P-driven signaling in non-Hodgkin lymphoma. *Blood Cancer J.* **8**, 97 (2018).
35. V. N. Ngo, R. M. Young, R. Schmitz, S. Jhavar, W. Xiao, K. H. Lim, H. Kohlhammer, W. Xu, Y. Yang, H. Zhao, A. L. Shaffer, P. Romesser, G. Wright, J. Powell, A. Rosenwald, H. K. Muller-Hermelink, G. Ott, R. D. Gascoyne, J. M. Connors, L. M. Rimsza, E. Campo, E. S. Jaffe, J. Delabie, E. B. Smeland, R. I. Fisher, R. M. Braziel, R. R. Tubbs, J. R. Cook, D. D. Weisenburger, W. C. Chan, L. M. Staudt, Oncogenically active MYD88 mutations in human lymphoma. *Nature* **470**, 115–119 (2011).
36. E. E. Turer, R. M. Tavares, E. Mortier, O. Hitotsumatsu, R. Advincula, B. Lee, N. Shifrin, B. A. Malynn, A. Ma, Homeostatic MyD88-dependent signals cause lethal inflammation in the absence of A20. *J. Exp. Med.* **205**, 451–464 (2008).
37. O. C. Leeksma, N. F. de Miranda, H. Veelken, Germline mutations predisposing to diffuse large B-cell lymphoma. *Blood Cancer J.* **7**, e541 (2017).
38. S. Lina, H. Ya'nan, Y. Ying, W. Fengfan, H. Xin, R. Xiaoxia, F. Ying, Haploinsufficiency of A20 caused by a novel pathogenic missense variant of TNFAIP3 and successfully treated with anti-TNF and immunosuppressive therapies. *Cell. Immunol.* **391-392**, 104753 (2023).
39. N. Aslani, K. Asnaashari, N. Parvaneh, M. Shahrooei, M. Sotoudeh-Anvari, F. Shahram, V. Ziaee, TNFAIP3 mutation causing haploinsufficiency of A20 with a hemophagocytic lymphohistiocytosis phenotype: A report of two cases. *Pediatr. Rheumatol. Online J.* **20**, 78 (2022).
40. L. Zanatta, F. Biscaro, S. Bresolin, M. Marzaro, S. Sarcognato, I. Cataldo, A. Marzollo, S. Martelossi, Case report: An early-onset inflammatory colitis due to a variant in TNFAIP3 causing A20 haploinsufficiency. *Front. Pediatr.* **10**, 1044007 (2022).
41. T. Kadowaki, H. Ohnishi, N. Kawamoto, T. Hori, K. Nishimura, C. Kobayashi, T. Shigemura, S. Ogata, Y. Inoue, T. Kawai, E. Hiejima, M. Takagi, K. Imai, R. Nishikomori, S. Ito, T. Heike, O. Ohara, T. Morio, T. Fukao, H. Kanegane, Haploinsufficiency of A20 causes autoinflammatory and autoimmune disorders. *J. Allergy Clin. Immunol.* **141**, 1485–1488. e11 (2018).
42. P. K. Mattila, C. Feest, D. Depoil, B. Treanor, B. Montaner, K. L. Otipoby, R. Carter, L. B. Justement, A. Bruckbauer, F. D. Batista, The actin and tetraspanin networks organize receptor nanoclusters to regulate B cell receptor-mediated signaling. *Immunity* **38**, 461–474 (2013).
43. A. Cherukuri, T. Shoham, H. W. Sohn, S. Levy, S. Brooks, R. Carter, S. K. Pierce, The tetraspanin CD81 is necessary for partitioning of coligated CD19/CD21-B cell antigen receptor complexes into signaling-active lipid rafts. *J. Immunol.* **172**, 370–380 (2004).
44. G. Pavlasova, M. Mraz, The regulation and function of CD20: An "enigma" of B-cell biology and targeted therapy. *Haematologica* **105**, 1494–1506 (2020).
45. M. A. Gomes de Castro, H. Wildhagen, S. Sograte-Idrissi, C. Hitzing, M. Binder, M. Trepel, N. Engels, F. Opazo, Differential organization of tonic and chronic B cell antigen receptors in the plasma membrane. *Nat. Commun.* **10**, 820 (2019).
46. J. Ren, R. Qu, N. T. Rahman, J. M. Lewis, A. L. O. King, X. Liao, F. N. Mirza, K. R. Carlson, Y. Huang, S. Gigante, B. Evans, B. K. Rajendran, S. Xu, G. Wang, F. M. Foss, W. Damsky, Y. Kluger, S. Krishnaswamy, M. Girardi, Integrated transcriptome and trajectory analysis of cutaneous T-cell lymphoma identifies putative precancer populations. *Blood Adv.* **7**, 445–457 (2023).
47. N. Borcherding, A. P. Voigt, V. Liu, B. K. Link, W. Zhang, A. Jabbari, Single-cell profiling of cutaneous T-cell lymphoma reveals underlying heterogeneity associated with disease progression. *Clin. Cancer Res.* **25**, 2996–3005 (2019).
48. C. Murga-Zamalloa, R. A. Wilcox, GATA-3 in T-cell lymphoproliferative disorders. *IUBMB Life* **72**, 170–177 (2020).
49. F. Vences-Catalan, C. C. Kuo, R. Rajapaksa, C. Duault, N. Andor, D. K. Czerwinski, R. Levy, S. Levy, CD81 is a novel immunotherapeutic target for B cell lymphoma. *J. Exp. Med.* **216**, 1497–1508 (2019).
50. O. L. Haigh, E. J. Grant, T. H. O. Nguyen, K. Kedzierska, M. A. Field, J. J. Miles, Genetic bias, diversity indices, physiochemical properties and CDR3 motifs divide auto-reactive from allo-reactive T-cell repertoires. *Int. J. Mol. Sci.* **22**, 1625 (2021).
51. J. Petersen, V. Montserrat, J. R. Mujico, K. L. Loh, D. X. Beringer, M. van Lummel, A. Thompson, M. L. Mearin, J. Schweizer, Y. Kooy-Winkelaar, J. van Bergen, J. W. Drijfhout, W. T. Kan, N. L. La Gruta, R. P. Anderson, H. H. Reid, F. Koning, J. Rossjohn, T-cell receptor recognition of HLA-DQ2-gliadin complexes associated with celiac disease. *Nat. Struct. Mol. Biol.* **21**, 480–488 (2014).
52. C. Schultheiss, D. Simnica, E. Willscher, A. Oberle, L. Fanchi, N. Bonzanni, N. H. Wildner, J. S. Z. Wiesch, C. Weiler-Normann, A. W. Lohse, M. Binder, Next-generation immunosequencing reveals pathological T-cell architecture in autoimmune hepatitis. *Hepatology* **73**, 1436–1448 (2021).
53. M. Werner, S. Almer, H. Prytz, S. Lindgren, S. Wallerstedt, E. Bjornsson, A. Bergquist, H. Sandberg-Gertzen, R. Hultcrantz, P. Sangfelt, O. Weiland, A. Danielsson, Hepatic and extrahepatic malignancies in autoimmune hepatitis. A long-term follow-up in 473 Swedish patients. *J. Hepatol.* **50**, 388–393 (2009).
54. A. E. Pugh-Bernard, G. J. Silverman, A. J. Cappione, M. E. Villano, D. H. Ryan, R. A. Insel, I. Sanz, Regulation of inherently autoreactive VH4-34 B cells in the maintenance of human B cell tolerance. *J. Clin. Invest.* **108**, 1061–1070 (2001).
55. J. N. Schickel, S. Glauzy, Y. S. Ng, N. Chamberlain, C. Massad, I. Isnardi, N. Katz, G. Uzel, S. M. Holland, C. Picard, A. Puel, J. L. Casanova, E. Meffre, Self-reactive VH4-34-expressing IgG B cells recognize commensal bacteria. *J. Exp. Med.* **214**, 1991–2003 (2017).
56. M. E. Van Gijn, I. Ceccherini, Y. Shinar, E. C. Carbo, M. Slofstra, J. I. Arostegui, G. Sarrabay, D. Rowczenio, E. Omoyimni, B. Balci-Peynircioglu, H. M. Hoffman, F. Milhavet, M. A. Swertz, I. Touitou, New workflow for classification of genetic variants' pathogenicity applied to hereditary recurrent fevers by the International Study Group for Systemic Autoinflammatory Diseases (INSAID). *J. Med. Genet.* **55**, 530–537 (2018).
57. S. Schliffke, A. Carambia, N. Akyuz, B. Thiele, J. Herkel, M. Binder, T-cell repertoire profiling by next-generation sequencing reveals tissue migration dynamics of TRBV13-family clonotypes in a common experimental autoimmune encephalomyelitis mouse model. *J. Neuroimmunol.* **332**, 49–56 (2019).
58. A. Oberle, A. Brandt, M. Voigtlaender, B. Thiele, J. Radloff, A. Schulenkorf, M. Alawi, N. Akyüz, M. März, C. T. Ford, A. Krohn-Grimberghe, M. Binder, Monitoring multiple myeloma by next-generation sequencing of V(D)J rearrangements from circulating myeloma cells and cell-free myeloma DNA. *Haematologica* **102**, 1105–1111 (2017).
59. D. A. Bolotin, S. Poslavsky, I. Mitrophanov, M. Shugay, I. Z. Mamedov, E. V. Putintseva, D. M. Chudakov, MiXCR: Software for comprehensive adaptive immunity profiling. *Nat. Methods*, **12**, 380–381(2015).
60. V. I. Nazarov, M. V. Pogorelyy, E. A. Komech, I. V. IZvyagin, D. A. Bolotin, M. Shugay, D. M. Chudakov, Y. B. Lebedev, & I. Z. Mamedov, tcR: An R package for T cell receptor repertoire advanced data analysis. *BMC Bioinformatics* **16**, 175 (2015).
61. S. Dray, A.-B. Dufour, Theade4Package: Implementing the duality diagram for ecologists. *J. Stat. Soft.* **22**, 1–20 (2007).
62. tidyverse: Easily Install and Load the 'Tidyverse'; https://cran.r-project.org/package=tidyverse.
63. I. Kirsch, M. Vignali, H. Robin, T-cell receptor profiling in cancer. *Mol. Oncol.* **9**, 2063–2070 (2015).
64. E. C. Pielou, Species-diversity and pattern-diversity in the study of ecological succession. *J. Theor. Biol.*, **10**, 370–383 (1996).
65. E. Cerami, J. Gao, U. Dogrusoz, B. E. Gross, S. O. Sumer, B. A. Aksoy, A. Jacobsen, C. J. Byrne, M. L. Heuer, E. Larsson, Y. Antipin, B. Reva, A. P. Goldberg, C. Sander, N. Schultz, The cBio cancer genomics portal: An open platform for exploring multidimensional cancer genomics data. *Cancer Discov.* **2**, 401–404 (2012).
66. C. Xu, X. Gu, R. Padmanabhan, Z. Wu, Q. Peng, J. DiCarlo, Y. Wang, smCounter2: An accurate low-frequency variant caller for targeted sequencing data with unique molecular identifiers. *Bioinformatics* **35**, 1299–1309 (2019).
67. P. Danecek, J. K. Bonfield, J. Liddle, J. Marshall, V. Ohan, M. O. Pollard, A. Whitwham, T. Keane, S. A. McCarthy, R. M. Davies, H. Li, Twelve years of SAMtools and BCFtools. *Gigascience* **10**, giab008 (2021).
68. J. Ye, N. Ma, T. L. Madden, J. M. Ostell, IgBLAST: An immunoglobulin variable domain sequence analysis tool. *Nucleic Acids Res.* **41**, W34–W40 (2013).
69. K. Wang, M. Li, H. Hakonarson, ANNOVAR: Functional annotation of genetic variants from high-throughput sequencing data. *Nucleic Acids Res.* **38**, e164 (2010).
70. K. Weber, U. Bartsch, C. Stocking, B. Fehse, A multicolor panel of novel lentiviral "gene ontology" (LeGO) vectors for functional gene analysis. *Mol. Ther.* **16**, 698–706 (2008).
71. M. I. Love, W. Huber, S. Anders, Moderated estimation of fold change and dispersion for RNA-seq data with DESeq2. *Genome Biol.* **15**, 550 (2014).
72. M. Stephens, False discovery rates: A new deal. *Biostatistics* **18**, 275–294 (2017).
73. S. Durinck, P. T. Spellman, E. Birney, W. Huber, Mapping identifiers for the integration of genomic datasets with the R/Bioconductor package biomaRt. *Nat. Protoc.* **4**, 1184–1191 (2009).
74. E. Y. Chen, C. M. Tan, Y. Kou, Q. Duan, Z. Wang, G. V. Meirelles, N. R. Clark, A. Ma'ayan, Enrichr: Interactive and collaborative HTML5 gene list enrichment analysis tool. *BMC Bioinformatics* **14**, 128 (2013).
75. C. Schultheiß, L. Paschold, E. Willscher, D. Simnica, A. Wöstemeier, F. Muscate, M. Wass, S. Eisenmann, J. Dutzmann, G. Keyßer, N. Gagliani, M. Binder, Maturation trajectories and transcriptional landscape of plasmablasts and autoreactive B cells in COVID-19. *iScience* **24**, 103325 (2021).

76. Y. Hao, S. Hao, E. Andersen-Nissen, W. M. Mauck, S. Zheng, A. Butler, M. J. Lee, A. J. Wilk, C. Darby, M. Zager, P. Hoffman, M. Stoeckius, E. Papalexi, E. P. Mimitou, J. Jain, A. Srivastava, T. Stuart, L. M. Fleming, B. Yeung, A. J. Rogers, J. M. McElrath, C. A. Blish, R. Gottardo, P. Smibert, R. Satija, Integrated analysis of multimodal single-cell data. *Cell* **184**, 3573–3587.e29 (2021).
77. E. Stephenson, G. Reynolds, R. A. Botting, F. J. Calero-Nieto, M. D. Morgan, Z. K. Tuong, K. Bach, W. Sungnak, K. B. Worlock, M. Yoshida, N. Kumasaka, K. Kania, J. Engelbert, B. Olabi, J. S. Spegarova, N. K. Wilson, N. Mende, L. Jardine, L. C. S. Gardner, I. Goh, D. Horsfall, J. McGrath, S. Webb, M. W. Mather, R. G. H. Lindeboom, E. Dann, N. Huang, K. Polanski, E. Prigmore, F. Gothe, J. Scott, R. P. Payne, K. F. Baker, A. T. Hanrath, I. C. D. S. van der Loeff, A. S. Barr, A. Sanchez-Gonzalez, L. Bergamaschi, F. Mescia, J. L. Barnes, E. Kilich, A. de Wilton, A. Saigal, A. Saleh, S. M. Janes, C. M. Smith, N. Gopee, C. Wilson, P. Coupland, J. M. Coxhead, V. Y. Kiselev, S. van Dongen, J. Bacardit, H. W. King; Cambridge Institute of Therapeutic Immunology and Infectious Disease-National Institute of Health Research (CITIID-NIHR) COVID-19 BioResource Collaboration, A. J. Rostron, A. J. Simpson, S. Hambleton, E. Laurenti, P. A. Lyons, K. B. Meyer, M. Z. Nikolić, C. J. A. Duncan, K. G. C. Smith, S. A. Teichmann, M. R. Clatworthy, J. C. Marioni, B. Göttgens, M. Haniffa, Single-cell multi-omics analysis of the immune response in COVID-19. *Nat. Med.* **27**, 904–916 (2021).
78. I. Korsunsky, N. Millard, J. Fan, K. Slowikowski, F. Zhang, K. Wei, Y. Baglaenko, M. Brenner, P. R. Loh, S. Raychaudhuri, Fast, sensitive and accurate integration of single-cell data with Harmony. *Nat. Methods* **16**, 1289–1296 (2019).
79. K. R. Moon, D. van Dijk, Z. Wang, S. Gigante, D. B. Burkhardt, W. S. Chen, K. Yim, A. V. D. Elzen, M. J. Hirn, R. R. Coifman, N. B. Ivanova, G. Wolf, S. Krishnaswamy, Visualizing structure and transitions in high-dimensional biological data. *Nat. Biotechnol.* **37**, 1482–1492 (2019).
80. M. V. Kuleshov, M. R. Jones, A. D. Rouillard, N. F. Fernandez, Q. Duan, Z. Wang, S. Koplev, S. L. Jenkins, K. M. Jagodnik, A. Lachmann, M. G. McDermott, C. D. Monteiro, G. W. Gundersen, A. Ma'ayan, Enrichr: A comprehensive gene set enrichment analysis web server 2016 update. *Nucleic Acids Res.* **44**, W90–W97 (2016).

Acknowledgments: We thank C. Wosiek, A. Patzschke, K. Nerger, Y. Du, K. Koerber-Ferl, and M. Siedlecki for excellent technical assistance. We thank A. Belot (Mère-Enfant Hospital Lyon, France), S. Aggoune (University of Algiers, Algeria), I. Touitou (University of Montpellier, France), and T. Roider (University of Heidelberg, Germany) for help with patient recruitment. The triple knockout (TKO) cell line and the vectors pMIZCC, pMIZYN, pMIZCC-BCR53, pMIZYN-BCR53, and pMICD8 were gifted by H. Jumaa and M. Dühren-von Minden (University Medical Center Ulm, Germany). We would also like to thank A. Navarrete-Santos and the cell sorting core facility at the Martin-Luther-University Halle-Wittenberg as well as G. El Kassem and M. Böttcher (Martin-Luther-University Halle-Wittenberg) for assistance with the 10X Chromium Controller. Figures 1A and 5A were created with the help of BioRender.com. **Funding:** Financial support from the Deutsche Forschungsgemeinschaft (SFB841 and BI 1711/4-1 to M.B.) as well as Intramural Funding of the Research Program of the National Human Genome Research Institute (to I.A.) is acknowledged. This work was also funded by the Deutsche Forschungsgemeinschaft (DFG, German Research Foundation) – SFB 1648/1 2024 – 512741711 and the Swiss National Science Foundation (SNSF) [10.001.762] (both to M.B.). **Author contributions:** Conceptualization: M.B., C.S., I.A., and A.W. Resources: I.A., A.W., A.M.-V., J.I.A., G.B., C.d.M., T.H., B.G., B.M., W.K., P.T.O., K.G., F.C., S.D., A.F., and D.M.S. Methodology: C.S., A.N.M., and A.W. Investigation: C.S., L.P., A.N.M., M.E., Y.M.K., M.M., H.J., and N.C. Software: E.W. and P.S.-B. Visualization: C.S., L.P., and E.W. Funding acquisition: M.B. and I.A. Project administration: M.B. and C.S. Supervision: MB. Writing—original draft: C.S., M.B., and I.A. Writing—review and editing: all authors. **Competing interests:** The authors declare that they have no competing interests. **Data and materials availability:** The herein reported sequence dataset has been deposited at ArrayExpress accession E-MTAB-12485 and E-MTAB-12491. All other data needed to evaluate the conclusions in the paper are present in the paper and/or the Supplementary Materials.

Submitted 16 October 2023
Accepted 15 July 2024
Published 21 August 2024
10.1126/sciadv.adl3975